Seminar at the von Karman Institute for Fluid Dynamics
Aeronautic and Aerospace Department

Predictive Material Modeling (PMM) overview

SPARTA
Stochastic Parallel Rarefied-gas Time-accurate Analyzer

PuMA
Porous Microstructure Analysis

PATO
Porous-material Analysis Toolbox based on OpenFOAM

ARCHeS
ARC Heater Simulator

Presented by Jeremie Meurisse

Part of the Entry System Modeling (ESM) project

10/20/2020

PMM organization

MACRO-SCALE MODELING
ARCHeS & PATO

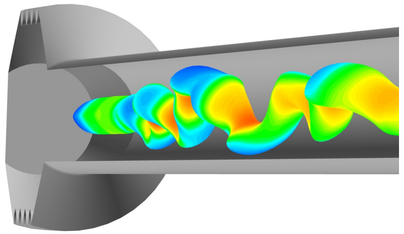
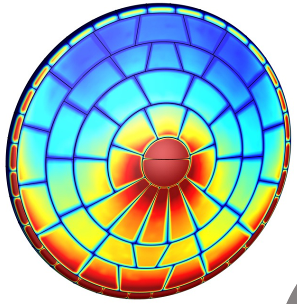

OPTIMIZATION, SA & UQ
Dakota

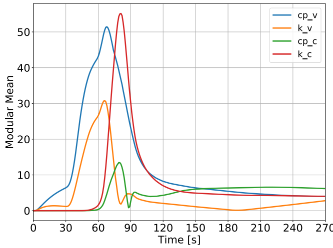

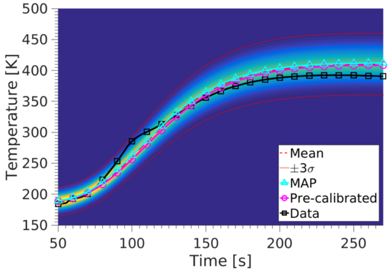

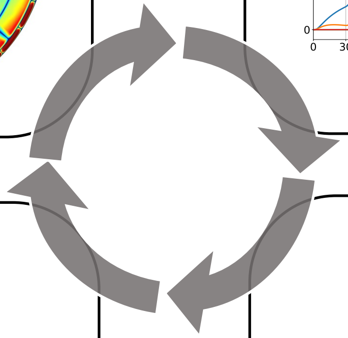

EXPERIMENTS
Verification & Validation

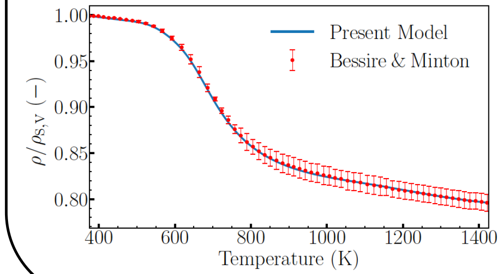

MICRO-SCALE MODELING
SPARTA & PuMA

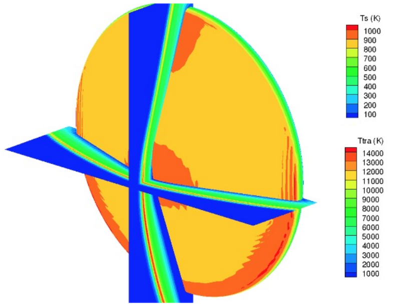
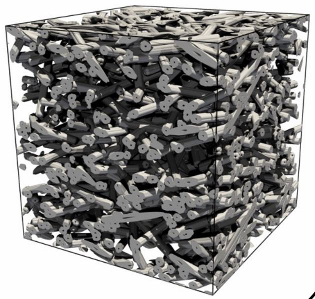

PMM Team

Arnaud Borner: Micro-scale lead and SPARTA developer.
Jeremie Meurisse: Macro-scale lead, ARCHeS and PATO developer.
Federico Semeraro: PuMA developer.
John Thornton: PuMA and PATO developer.
Krishnan Swaminathan Gopalan: Oxidation expert and PuMA developer.
Sergio Fraile Izquierdo: ARCHeS and PATO developer.
Patricia Ventura Diaz: CFD expert and DPLR user.
Georgios Bellas Chatzigeorgis: Material response expert and PATO developer.
Joshua Monk: Material response expert and PATO user.
Brody Bessire: Experimental design expert.
Magnus Haw: Experimental design expert.
Joseph Ferguson: PuMA developer.
Nagi Mansour: Former PMM task lead and senior advisor.

and many other collaborators, visiting scholars, and interns…

Mars Science Laboratory (MSL)

- MSL is a robotic space probe mission to Mars launched by NASA on November 26, 2011, which successfully landed Curiosity, a Mars rover, in Gale Crater on August 6, 2012.
- MSL was protected during Mars atmospheric entry by a 4.5 meter diameter heatshield, which was constructed by assembling 113 thermal tiles made of Phenolic Impregnated Carbon Ablator (PICA).

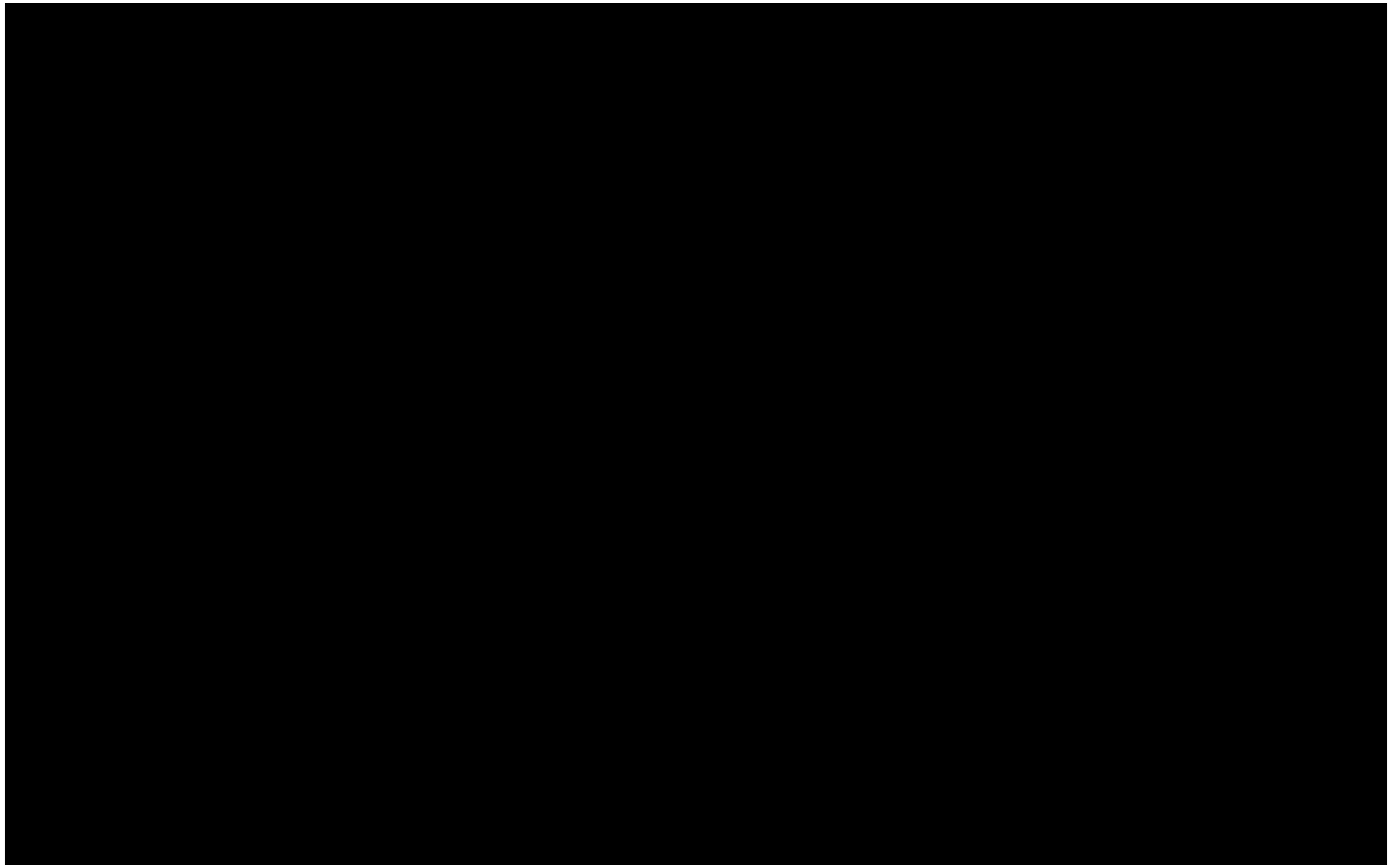

credit: NASA JPL

Porous Microstructure Analysis (PuMA) [1]

Porous Microstructure Analysis (PuMA)

Domain Generation

- X-ray Microtomography import / filtering
- Woven Material Generation (TexGen)
- Simplified Geometry Generation
  - Analytical shapes
  - Fibrous Materials
  - Sphere Beds
  - Triply Periodic Materials

Material Properties

- Porosity / Volume Fractions
- Specific Surface Area
- Pore Diameter
- Effective Thermal & Electrical Conductivity
- Anisotropic Thermal & Electrical Conductivity
- Anisotropic Elasticity
- Material Orientation
- Continuum Tortuosity
- Rarefied Tortuosity
- Permeability

Shared Utilities

- Matrix & Vector data structures / operations
- Linear Solvers
- Iso-surface extraction
- Input/output utilities

Material Response

- Microscale Oxidation
- Transient Diffusion
- Transient Conduction
- Hyperthermal Beam Simulations

● Included in V3 release
○ Not included in V3 release

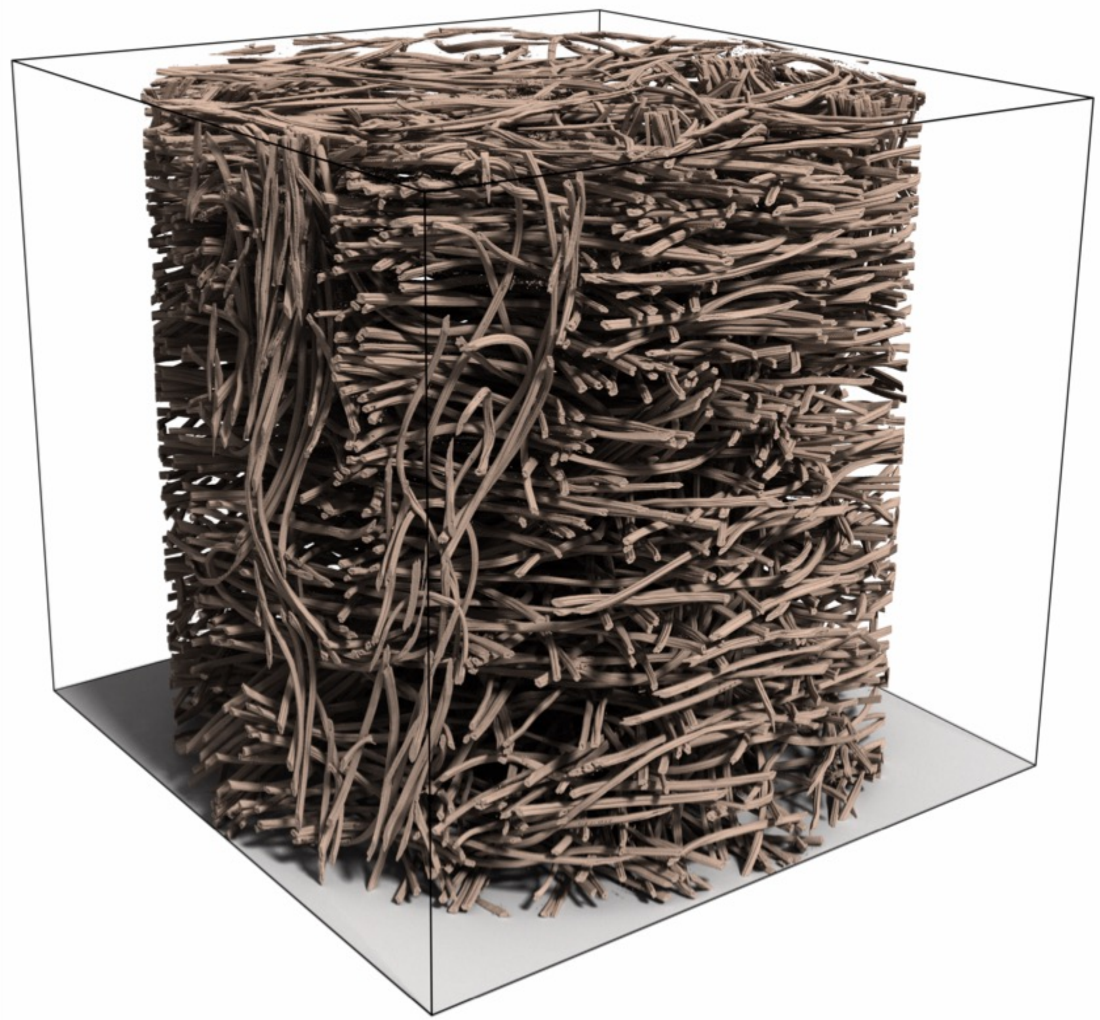

Transport Properties at the micro-scale

Effective Thermal Conductivity

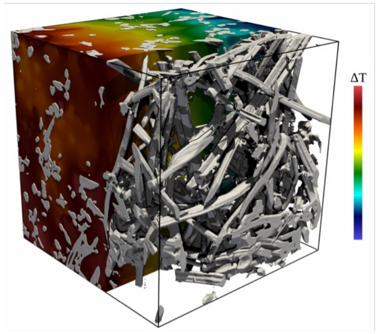

Conductivity of fibrous materials

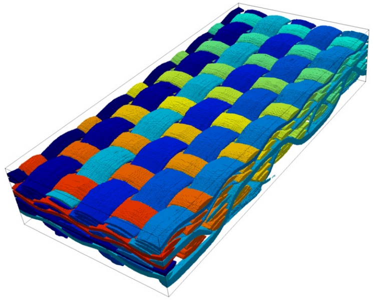

Woven materials considering anisotropy

Tortuosity / Diffusivity

High Knudsen

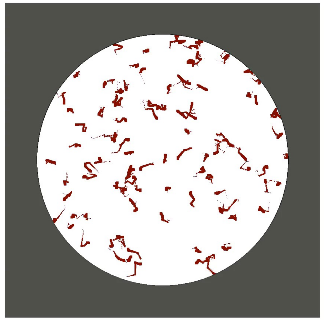

Low Knudsen

Permeability

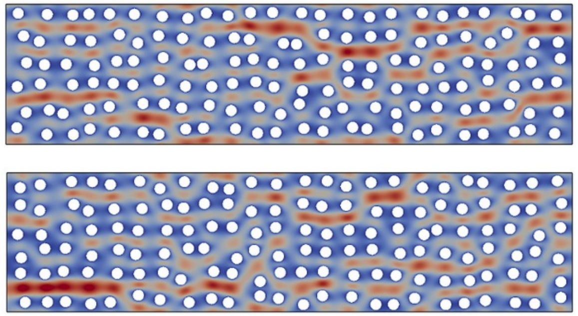

Pressure driven flow through 2D fibrous material

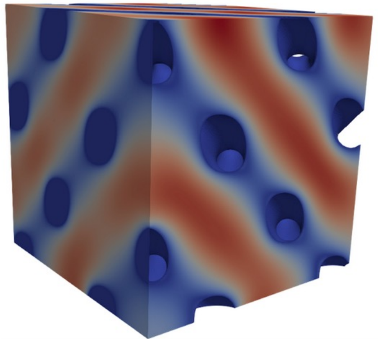

Pressure driven flow through 3D triply periodic material

Considering Anisotropy

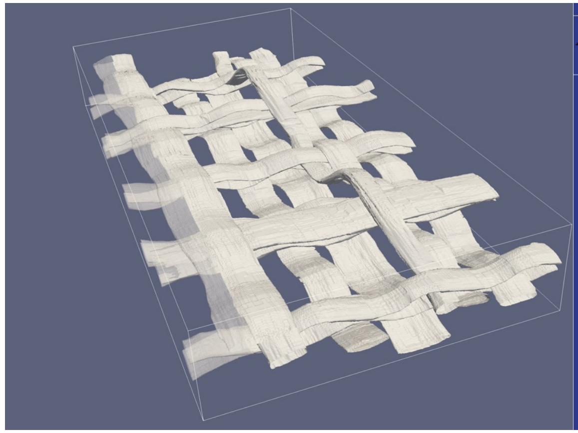

Ray casting direction estimation

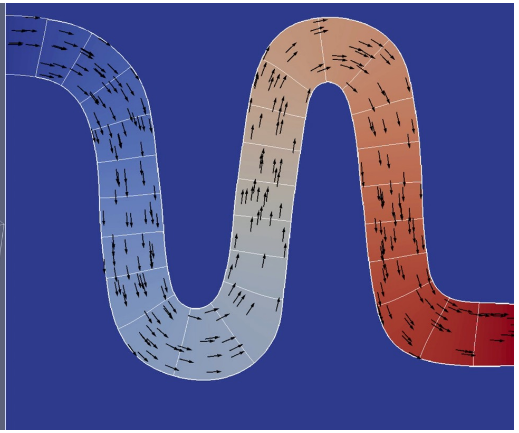

Heat flux direction estimation

Effective properties for fibrous media [2,3]

Fibers and weaves generator

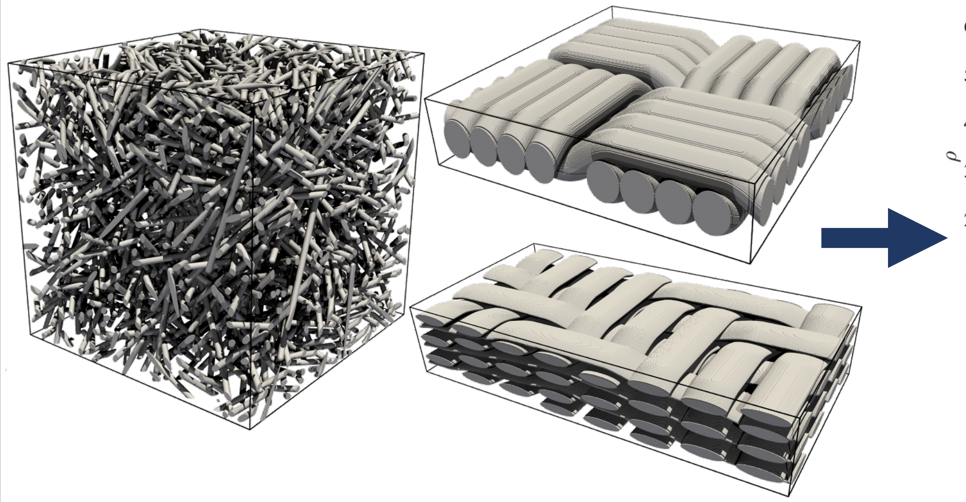

Fiber and weave orientation

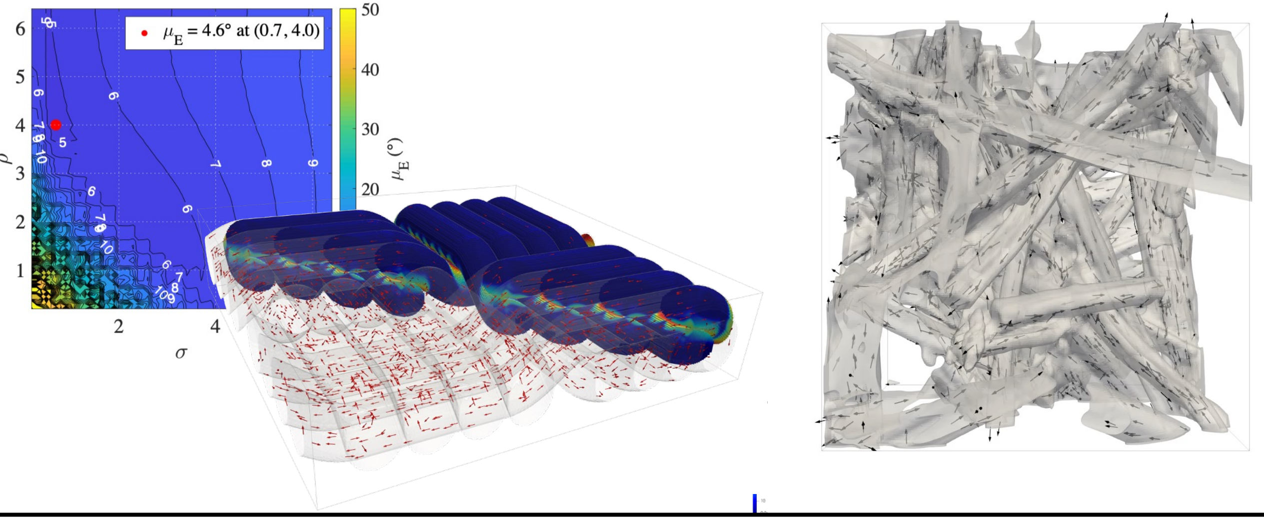

Effective thermal conductivity

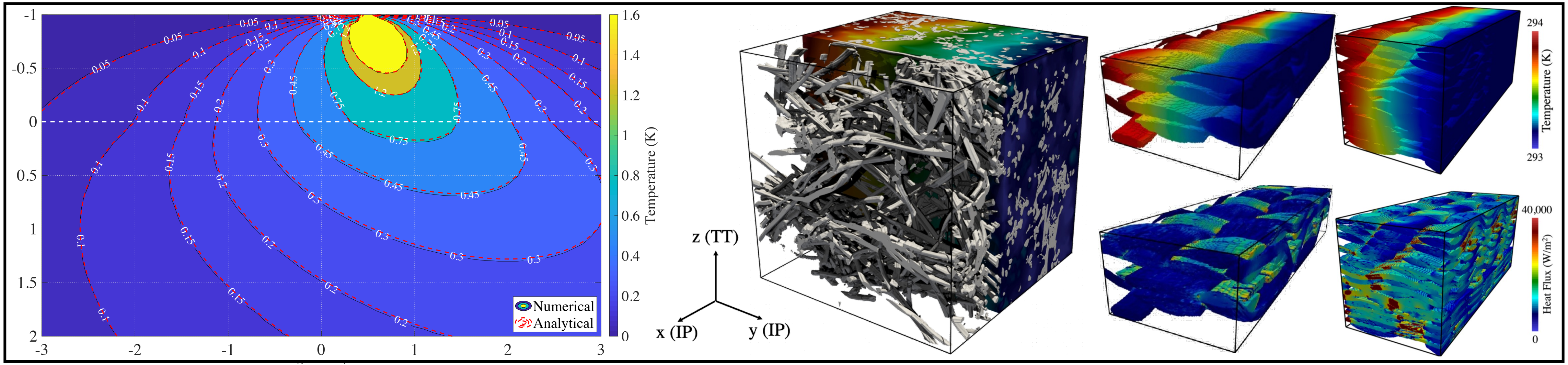

SPARTA (DSMC code) [4]

- Open-source DSMC solver initiated at SNL, currently co-developed by Sandia and NASA with multiple users internationally and domestically: https://sparta.sandia.gov
- Distributed-memory MPI, spatially decomposed domain
- Portable: C++ (really object-oriented C style)
- Can be run from single processor to petascale.
- 3D, 2D or 2D-axisymmetric domains
- Cartesian, hierarchical grid with multiple levels of refinement
- Gas phase collisions and chemistry
- Surface collisions and chemistry
- Has been used to run the largest (we think!) DSMC models up-to-date, with up to **100 billion particles and billions of grid cells**
- Embedded triangulated surfaces in grid (read from STL file)
- Code initially designed to handle **~100k** surface elements

Image credit: M. Gallis (Sandia)

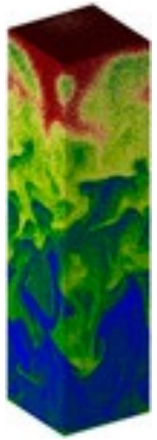

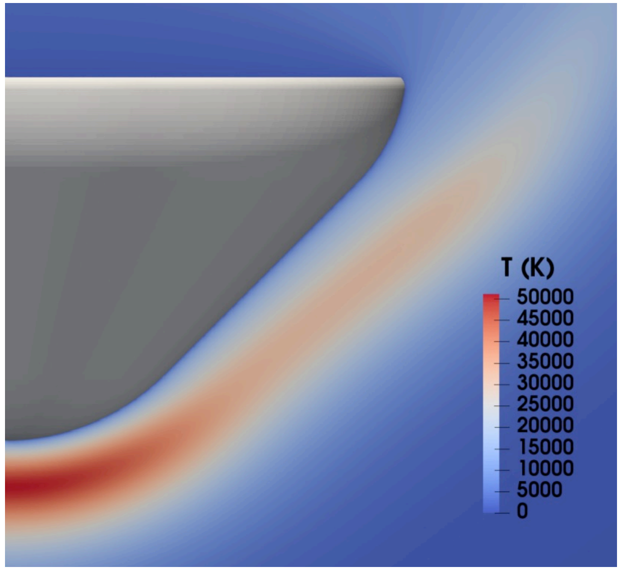

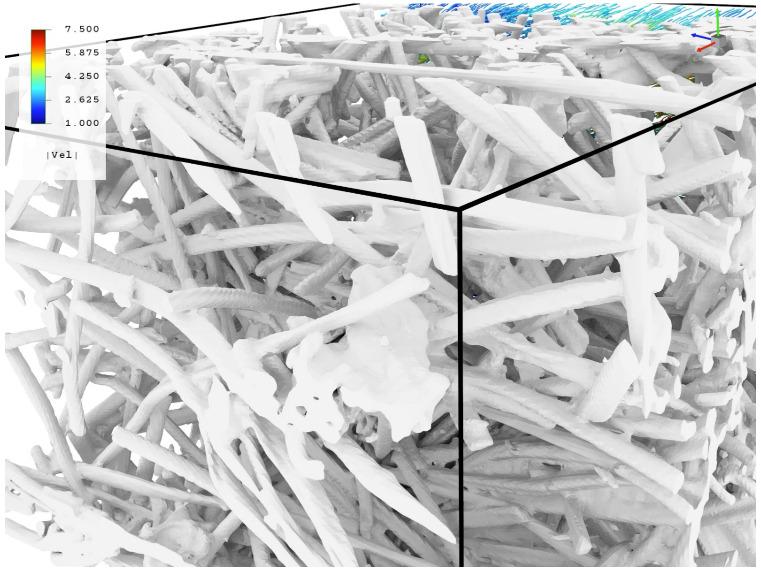

Ablation of Carbon Fiber TPS Samples in DSMC

- Implementation of a new surface generation model in SPARTA DSMC code (built from microtomography images)
- Implementation of ablation model
- Example:
  - 800^3 voxels sample = 512M grid cells
  - 57.6M surface elements, 60M particles, 22M surf collisions/step

- Benchmarking with many randomly generated surfaces:

Case (^3)	# grid cells	# tris	# Broadwell cores	read method	Total read-create time (s)	ablate time (s)	Memory total (GB)
200	**8.000E+06**	**2.537E+07**	**560**	**serial**	1.954	0.686	6.32
				parallel	0.846		
			1120	**serial**	1.929	0.373	
				parallel	0.689		
400	**6.400E+07**	**2.040E+08**	**560**	**serial**	15.722	4.66	50.7
				parallel	5.200		
			1120	**serial**	13.550	2.94	
				parallel	3.861		
800	**5.120E+08**	**1.636E+09**	**1120**	**serial**	105.748	25	406.03
				parallel	28.901		
			2240	**serial**	105.390	13.64	
				parallel	16.490		
1600	**4.096E+09**	**1.310E+10**	**7000**	**serial**	747.352	59	3249.65
				parallel	72.172		

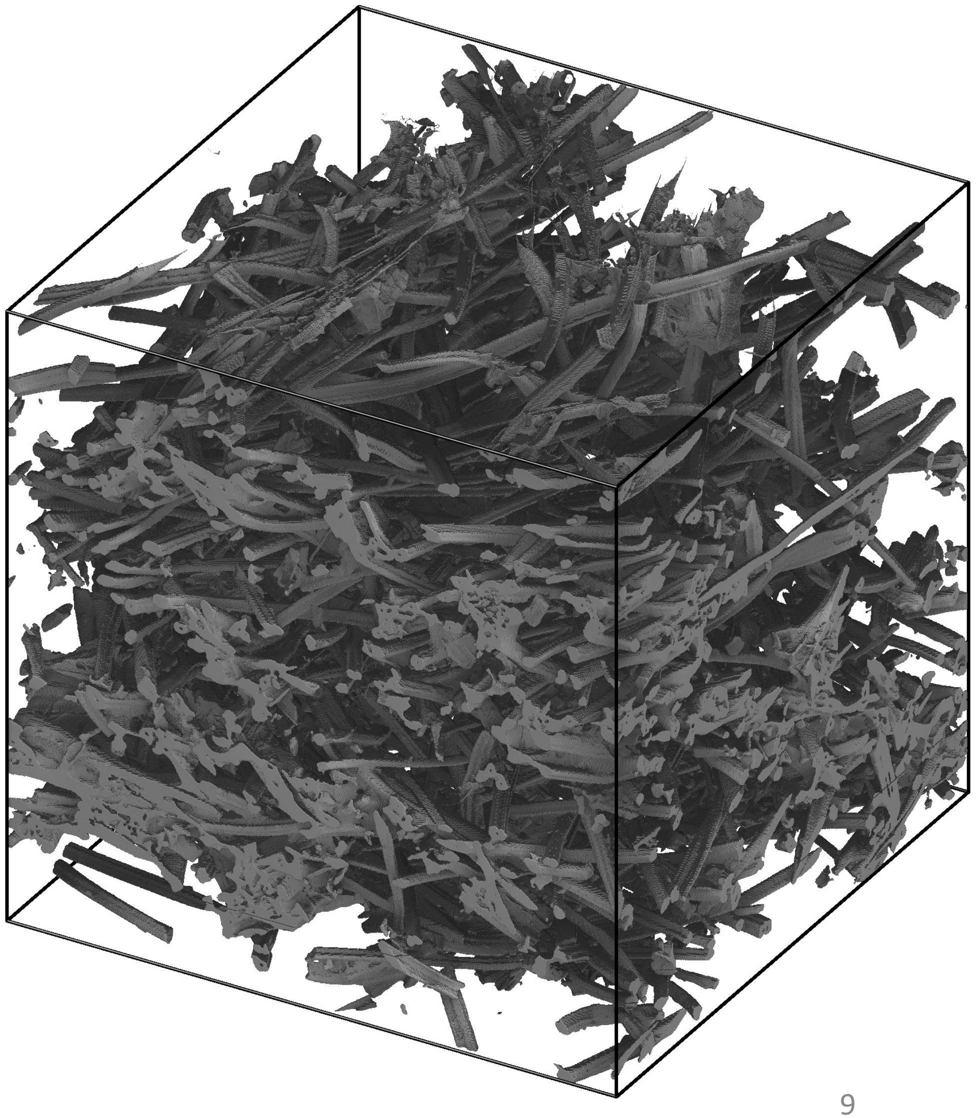

DSMC Simulations of Hypervelocity Sampling in Venus' Upper Atmosphere

- **Cupid's Arrow Mission Concept: Small probe designed to sample upper atmosphere of Venus and measure noble gas abundances (JPL led)**
- Ar/Xe/Kr/Ne/He are the noble gases, 2 isotopes of each
- Driving Objective:
  - Is the gas acquired by the sampling system at 110 km in the Venus atmosphere while traveling at 10.5 km/s representative of the free stream?
  - Can isotopic fractionation be quantified and accurately predicted?
- First DSMC simulation to resolve internal and external flow features, spanning multiple length and time scales.
- Longest 3D run was for 30s of flight time, resolving multiple molecular time scales (20,000 cores simulation).
- Storing many levels of adaptation (12) and many particles (Billions) has a memory cost. These simulations can easily require 200+ TB RAM.

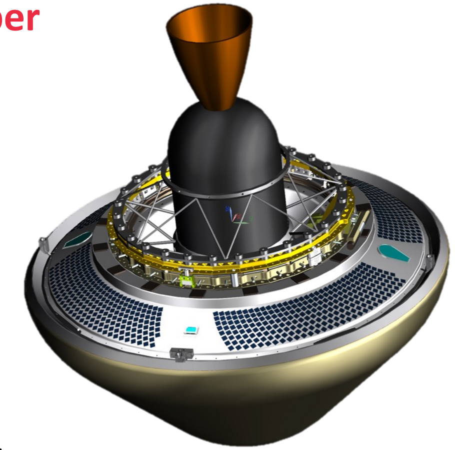

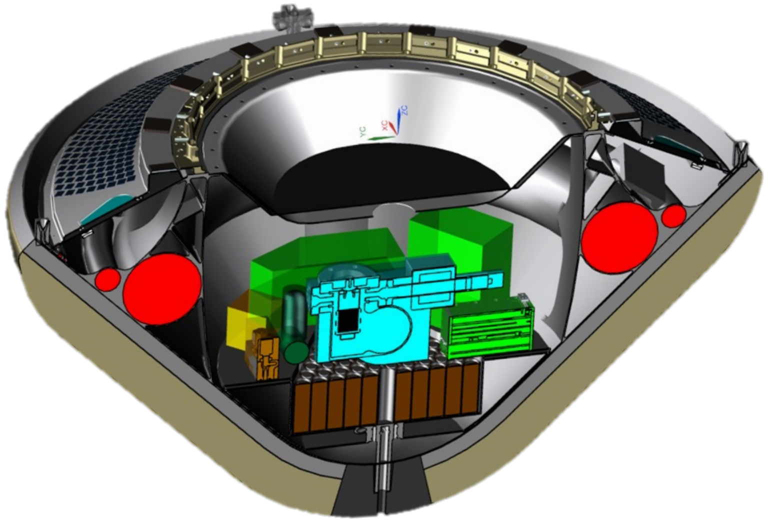

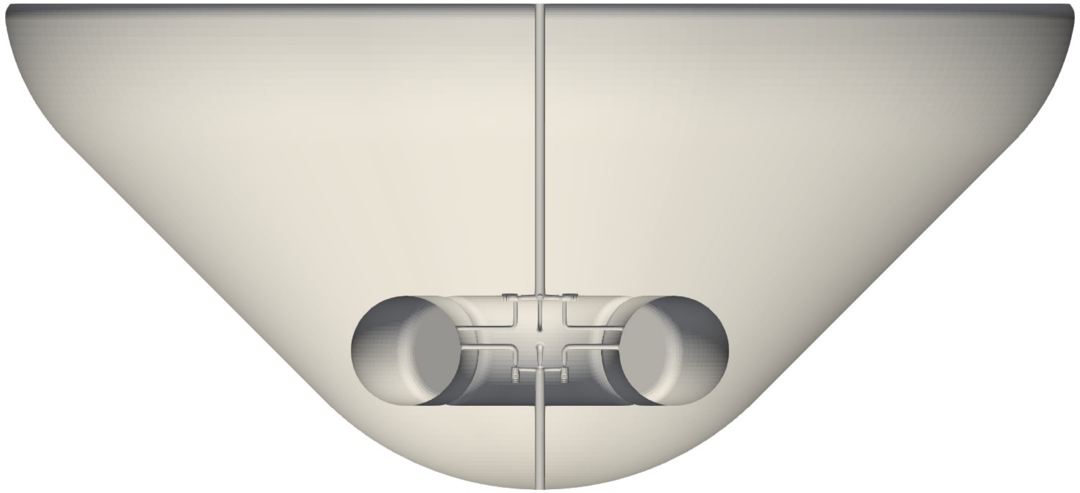

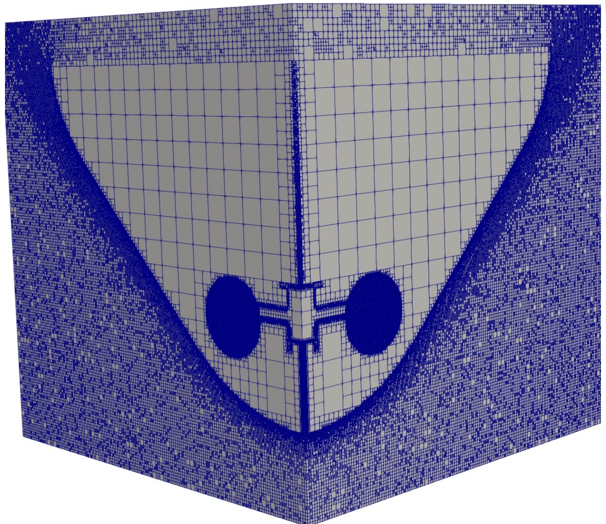

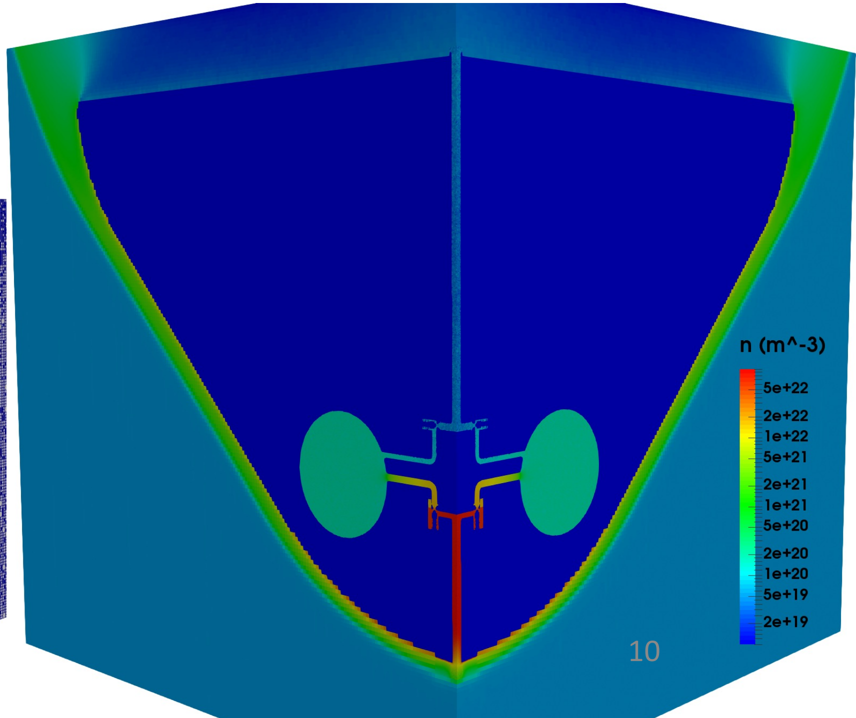

Porous material Analysis Toolbox based on OpenFOAM [5,6,7]

PATO overview

OpenFOAM

- Finite Volume
- PETSc
- I/O management
- Numerical schemes
- Massive MPI
- Fluid solvers
- Moving geometry
- Chemistry
- Basic mesh gen.
- Thermo/Transp.

PATO: material response

- *PATOx exectuable*
- *Pyrolysis*
- *libPATOx library*
- *Pure conduction*
- *Equilibrium chemistry*
- *1D/2D/3D mapping*
- *Finite-rate chemistry*
- *Multi-material*
- *Volume Ablation*
- *Fluid coupling*

Complex mesh generation

Thermo/Transport/ Chemistry

Optimization/ UQ/SA/PE

Post-processing 1D/2D/3D

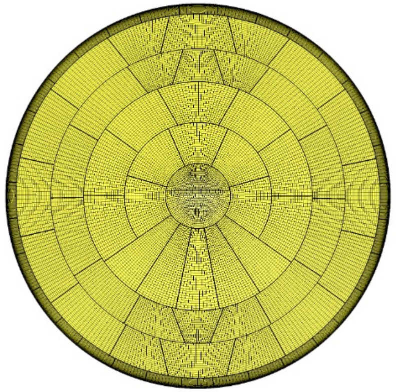

POINTWISE/GMSH

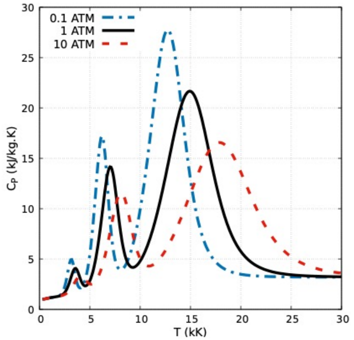

MUTATION++

DAKOTA

Explore and predict with confidence.

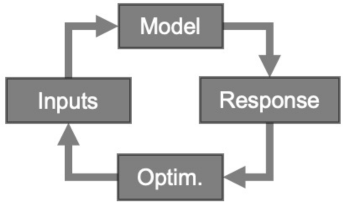

DAKOTA

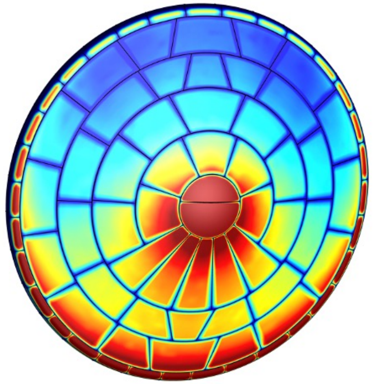

FV/TEC

More info on PATO

- *PATO website:*
  - http://www.pato.ac/
- *Private gitlab:*
  - gitlab.com/PATO/PATO-dev
- *PATO module on PFE*
  - module use -a /u/jmeuriss/modulefiles
  - module load PATO/dev
  - module load dakota/6.7
  - module load cmake/3.9
- *1D, 2D, 3D tutorials on PFE*
  - /u/jmeuriss/sharing/PATO/ PATO-dev/tutorials
- *Creators:*
  - *Jean Lachaud & Nagi Mansour*
- *Main developer:*
  - jeremie.b.meurisse@nasa.gov

MSL simulations using DPLR and PATO [7]

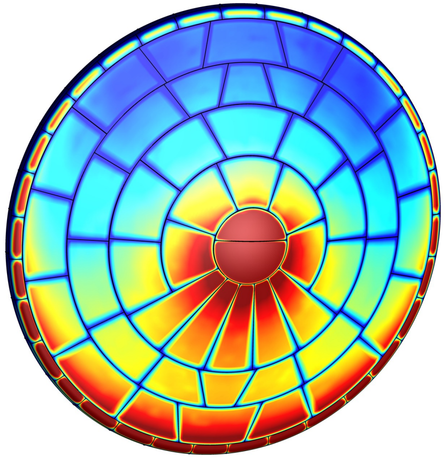

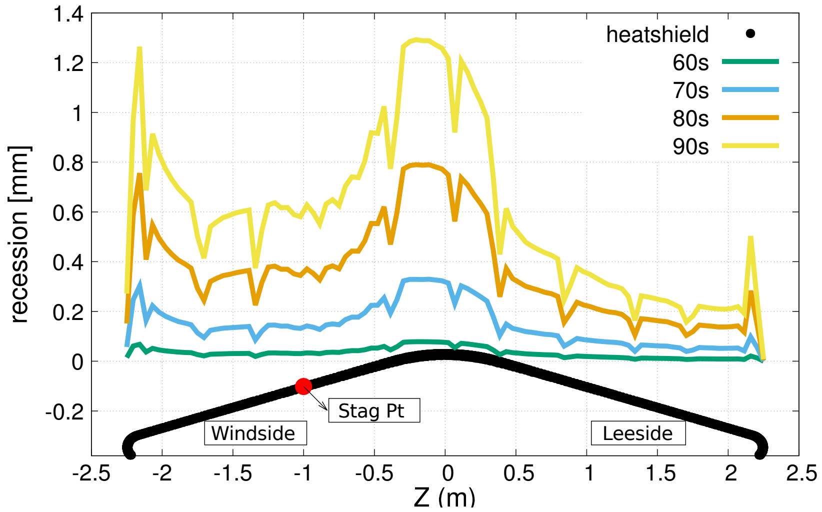

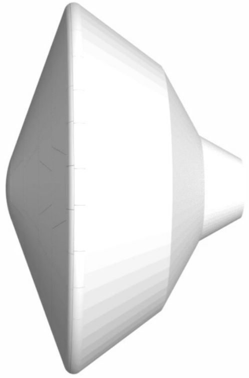

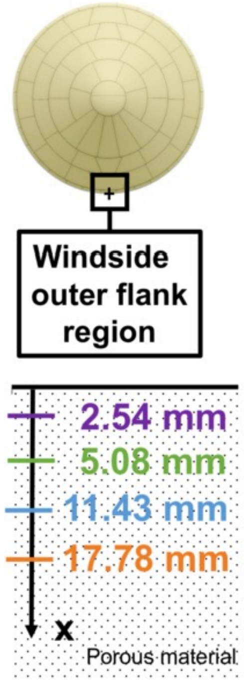

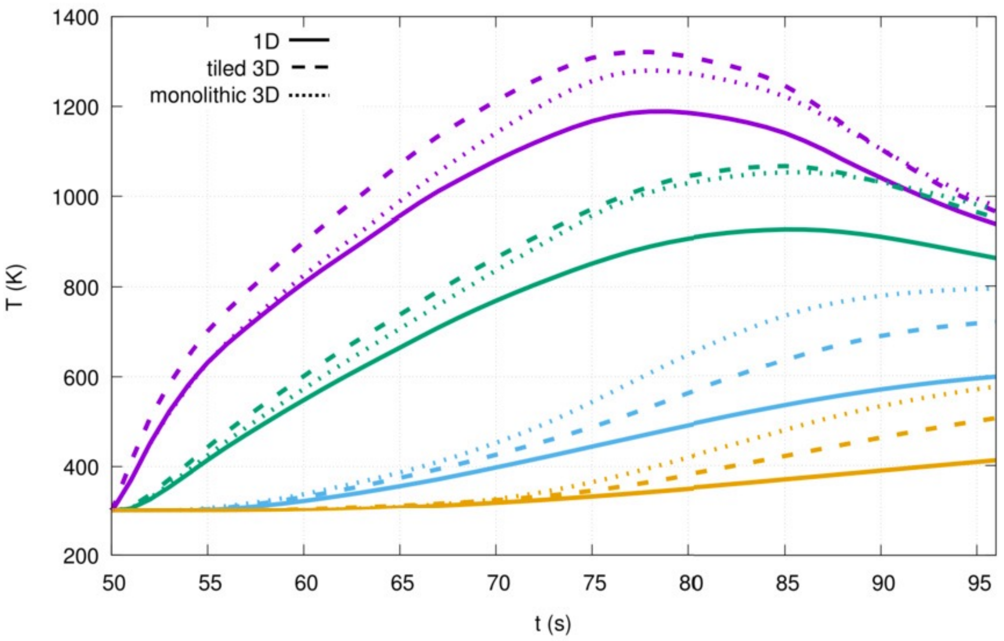

Fencing effect due to RTV between the tiles

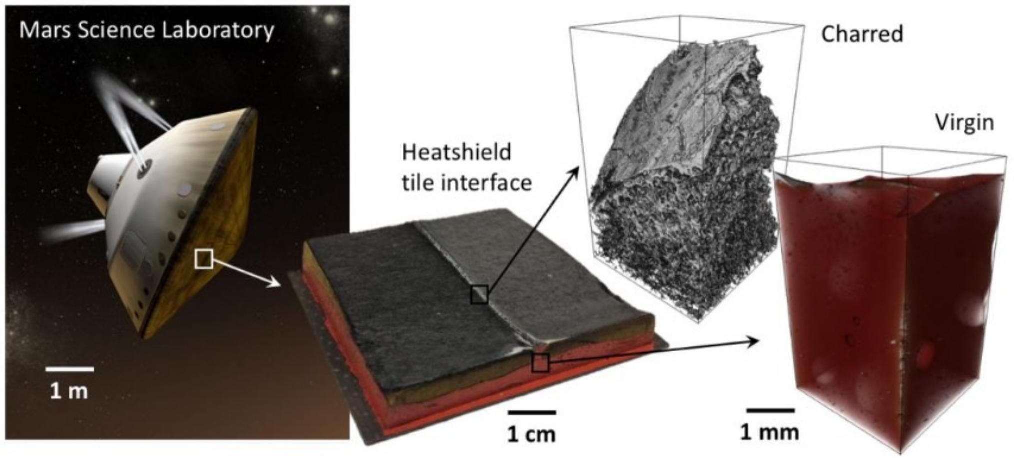

Calibration of the pyrolysis gases [8]

Oxygen

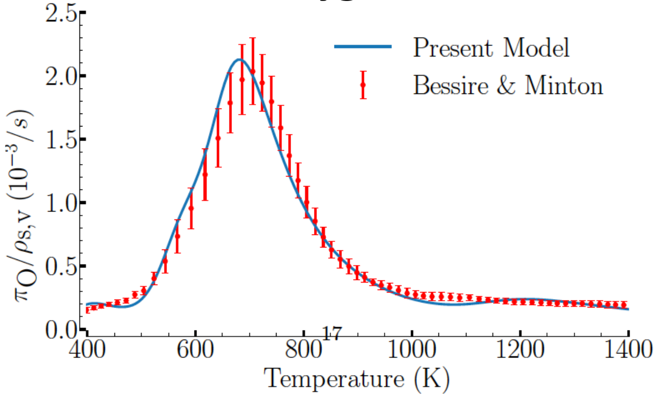

Hydrogen

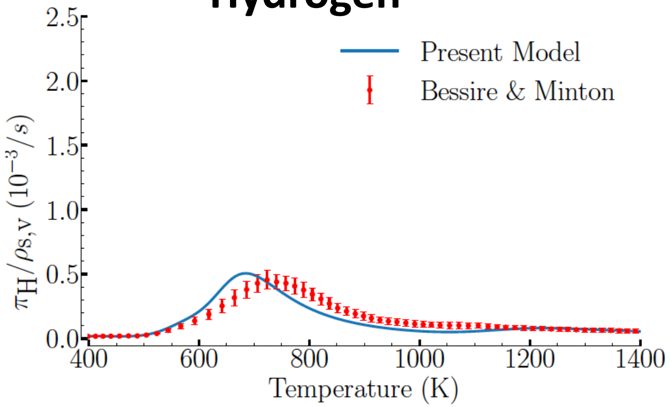

Carbon

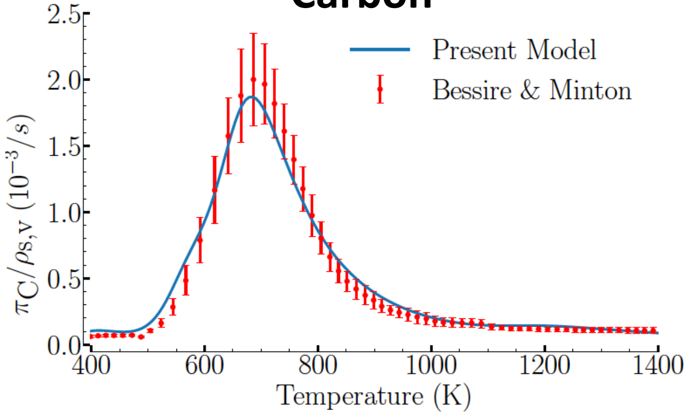

TGA curve

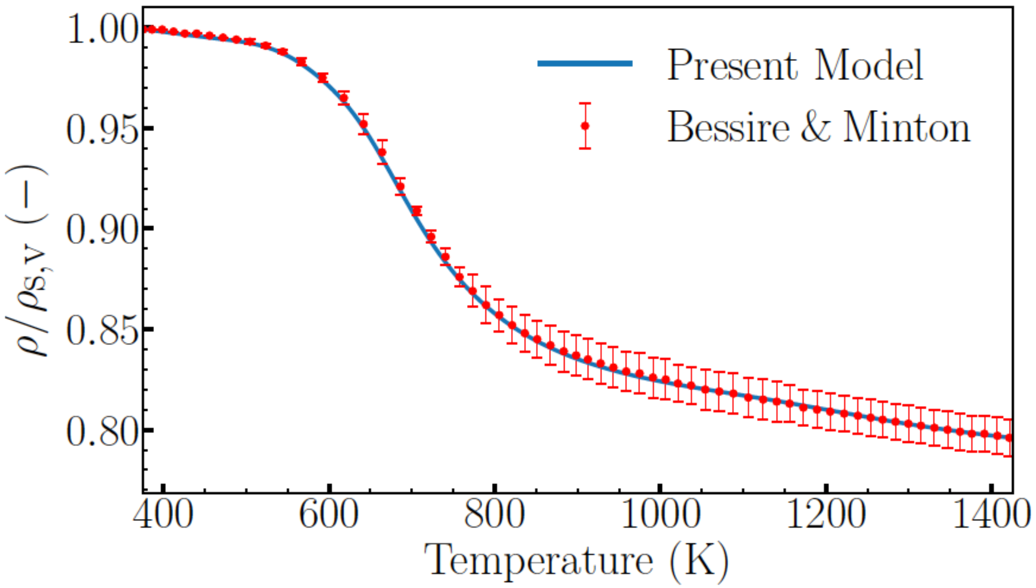

New pyrolysis model for PICA

R	F(-)	$\log(\mathcal{A})(s^{-1})$	$\mathcal{E}$(kJ/mol)	n (-)	ζ(-)	
1	0.032	5.67	51.4	7.74	C	0.32
					H	0.06
					O	0.62
2	0.089	7.02	87.4	4.02	C	0.40
					H	0.07
					O	0.53
3	0.336	7.03	103.7	4.33	C	0.42
					H	0.12
					O	0.46
4	0.086	6.9	194.4	9.25	C	0.25
					H	0.21
					O	0.54

Sensitivity analysis using Dakota and PATO

Environment (MISP2 – TC2)

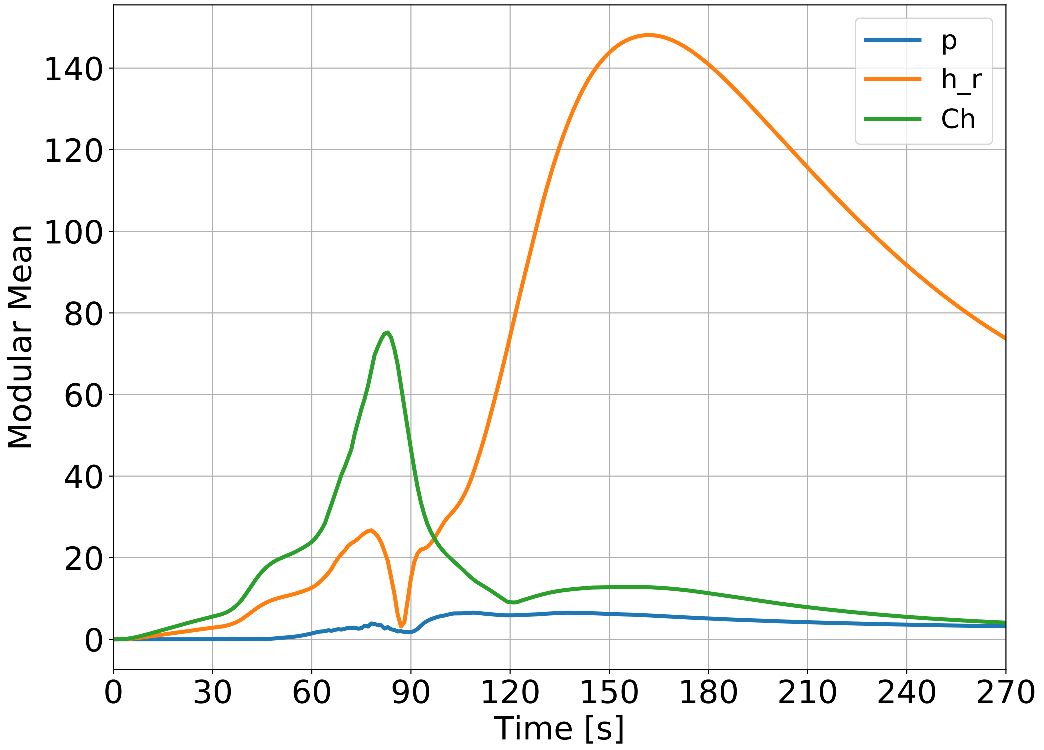

Material properties (MISP2 – TC2)

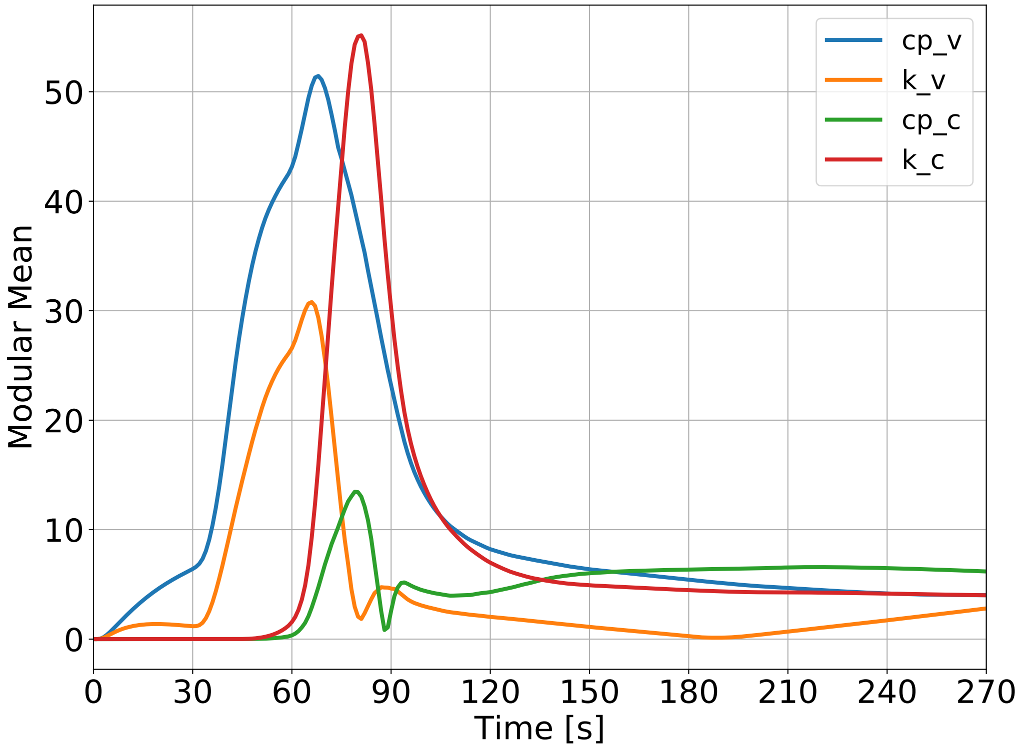

- Sensitivity of MSL response temperature to environment and material properties.
- Morris method in DAKOTA with PATO material response simulations for each MISP.
- Aerothermal environments obtained using DPLR (continuum) and SPARTA (rarefied).
- 1D material response simulations using PICA material properties.

High-fidelity modeling of the MSL heatshield entry

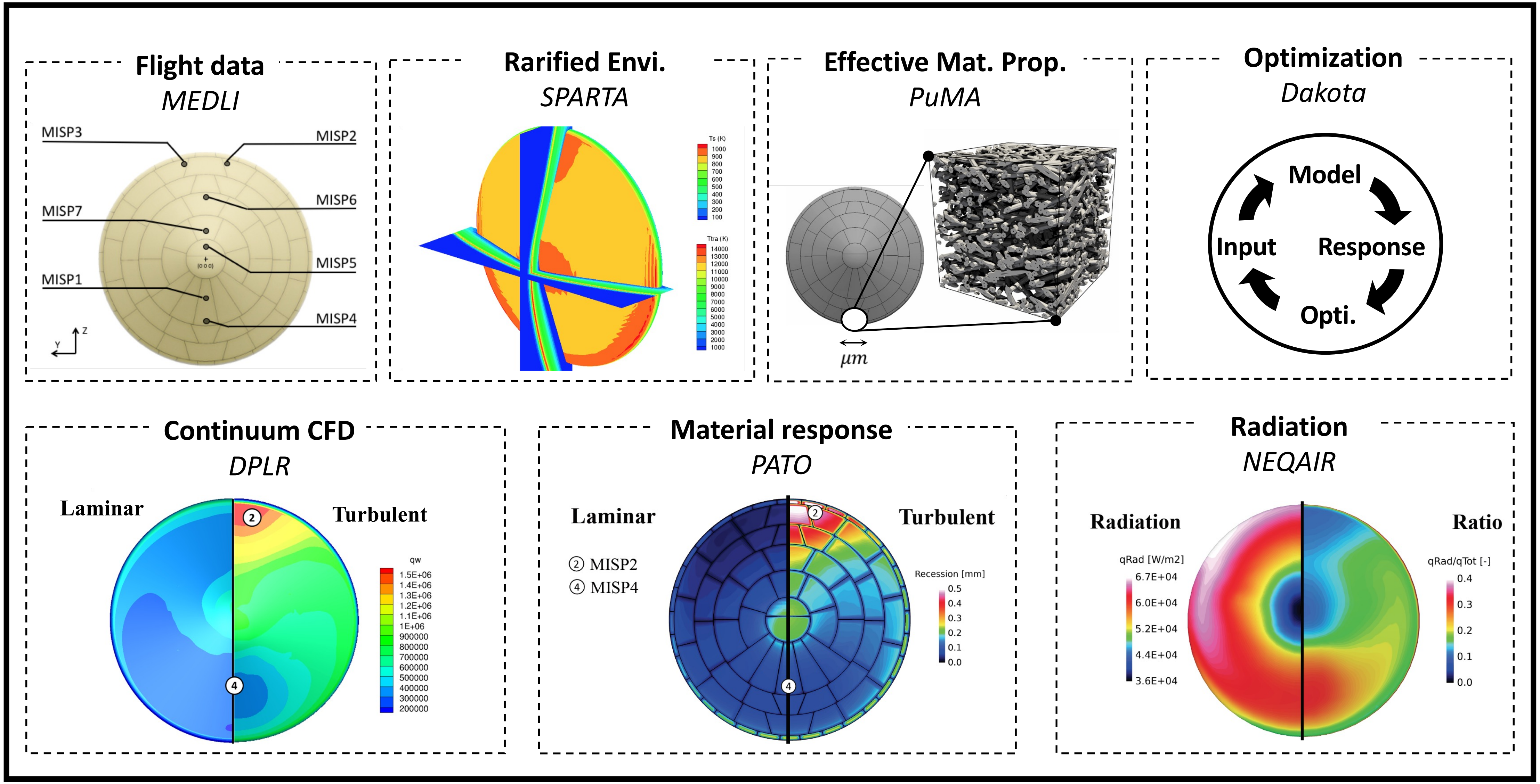

Arc-jets

- Arc-jets are essential facilities used in research, development and evaluation of Thermal Protection Systems (TPS) for hypersonic vehicles.
- Arc-jets produce high-enthalpy environments emulating atmospheric planetary entry.
- NASA's facilities:
    - NASA Ames Arc Jet Complex.
    - Hypersonic Materials Environmental Test System (HyMETS).

credit: NASA Ames

High-fidelity modeling of arc-jet testing

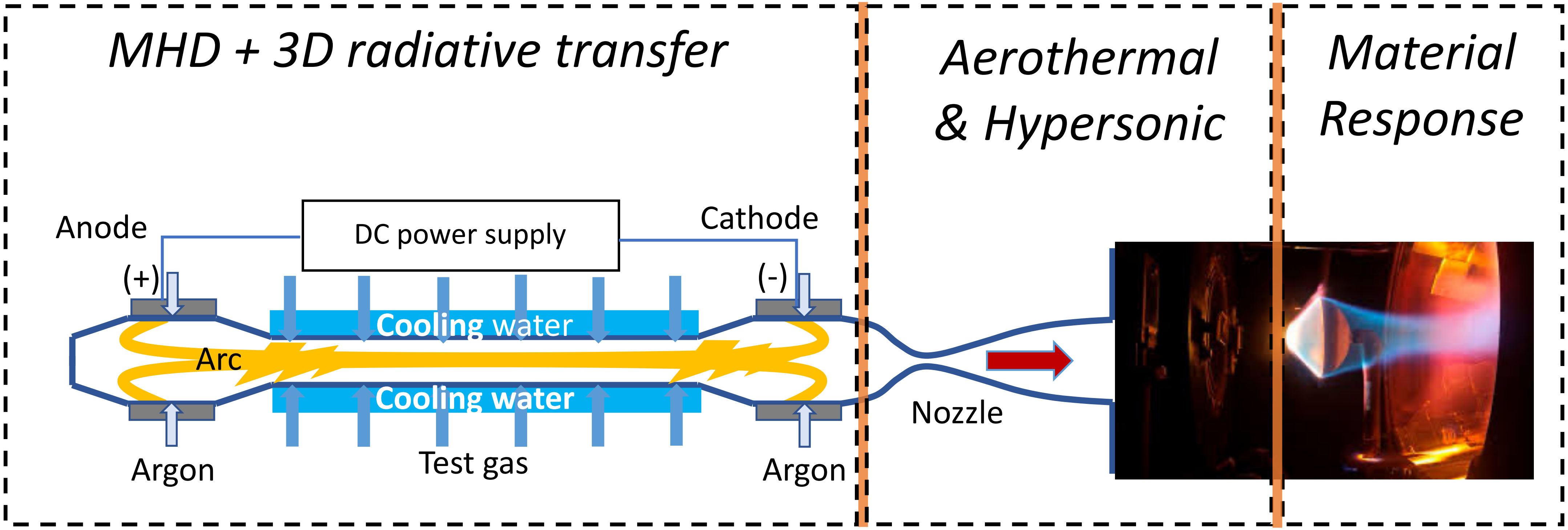

ARCHeS
ARCHeS
ARC Heater Simulator

DPLR
DPLR
Data-Parallel
Line Relaxation

PATO
Porous-material Analysis
Toolbox based on OpenFOAM

1st part of an arc-jet

High-fidelity modeling of arc heaters

MHD + 3D radiative transfer

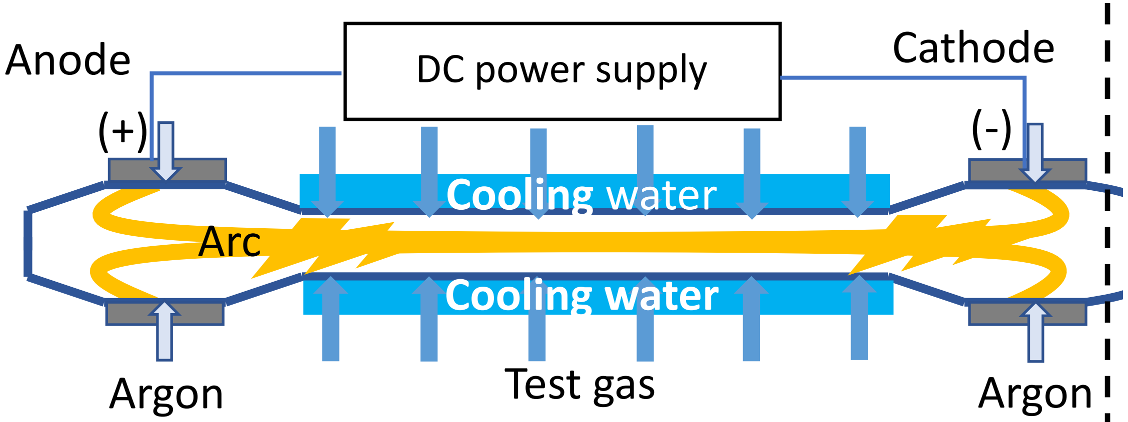

ARCHeS

ARC Heater Simulator

High-fidelity modeling of the **arc heaters**

Variable gas mixture

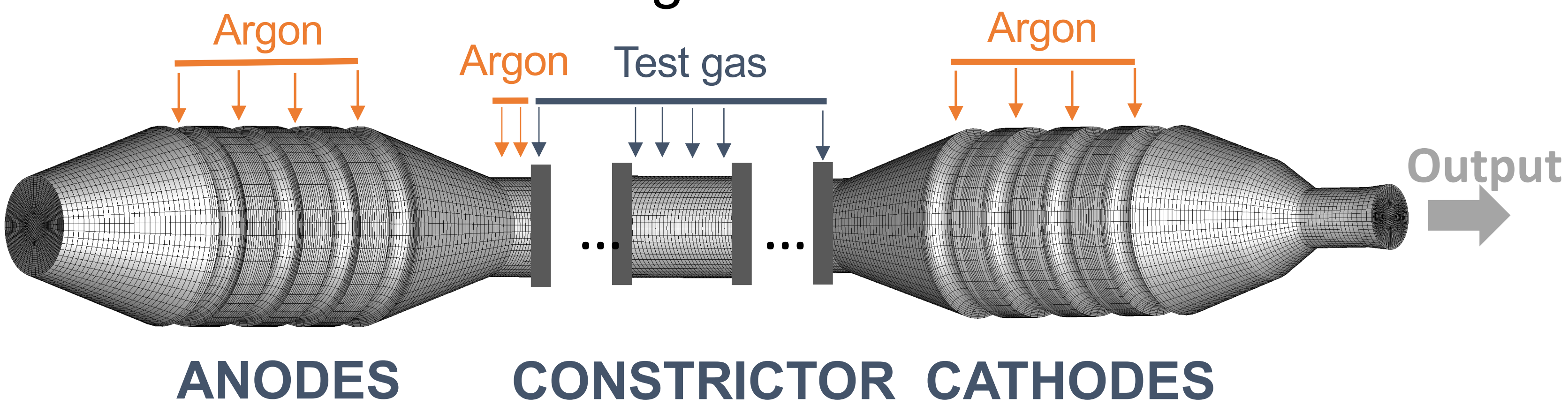

Swirl

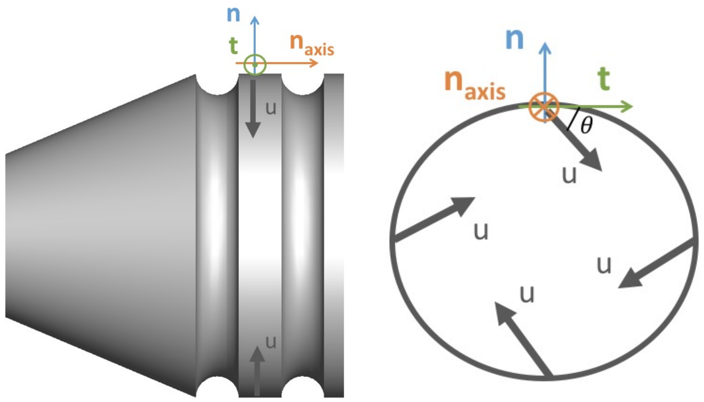

Internal magnetic drive

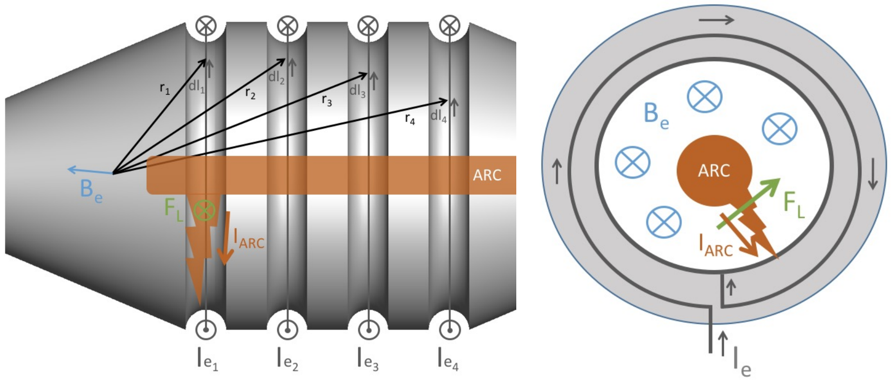

Electrical ballast

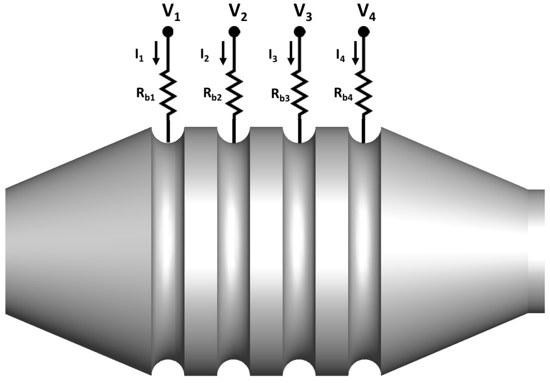

ARCHeS: ARC Heater Simulator [9]

Geometry concept

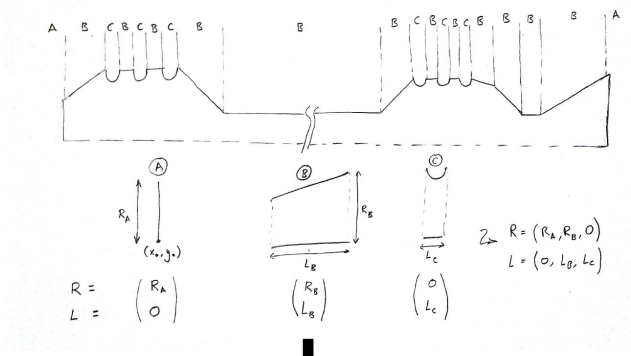

Automatic mesh inputs

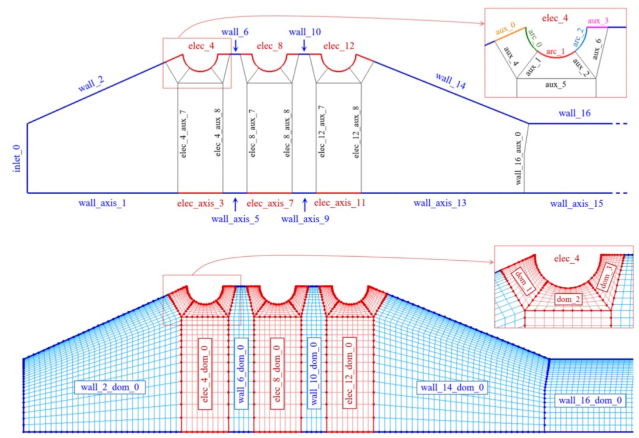

OpenFOAM

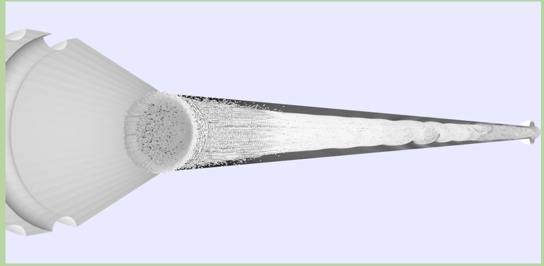

- Finite Volume
- I/O management
- Massive MPI
- Mixture tables
- Turbulence
- Moving geometry
- Chemistry
- Compressible flow
- Basic mesh gen.
- Thermo/Transp.
- Radiation

ARCHeS

MHD + ballast BC

3D radiative transfer

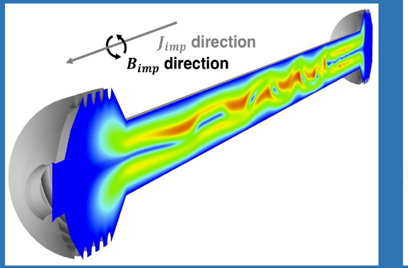

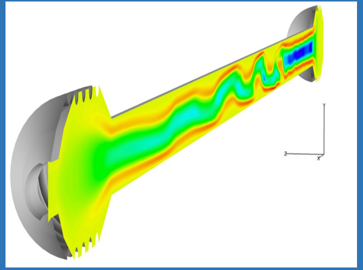

Complex mesh generation

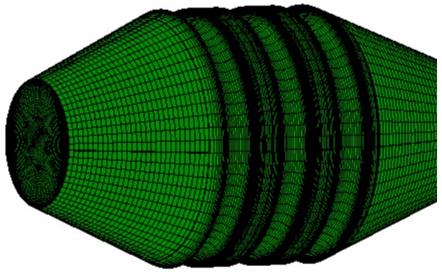

Thermo/Transport/ Chemistry

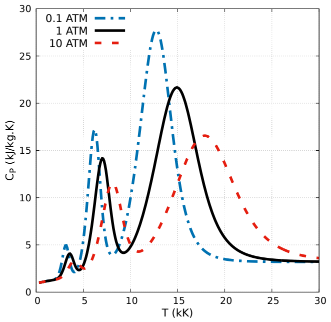

Post-processing 1D/2D/3D

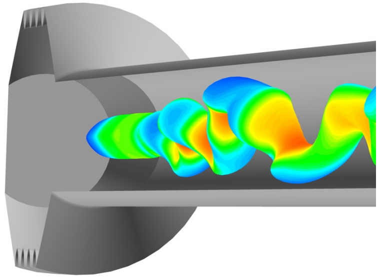

Multiphysics model

MASS	$\partial_t \rho + \boldsymbol{\partial}_\mathbf{x} . (\rho \mathbf{u}) = 0$
MOMENTUM	$\partial_t (\rho \mathbf{u}) + \boldsymbol{\partial}_\mathbf{x} . (\rho \mathbf{u}\mathbf{u}) = - \boldsymbol{\partial}_\mathbf{x} p + \boldsymbol{\partial}_\mathbf{x} . \bar{\bar{\boldsymbol{\tau}}} + \mathbf{J} \times \mathbf{B}$
ENERGY	$\partial_t (\rho E_0) + \boldsymbol{\partial}_\mathbf{x} . (\rho H_0 \mathbf{u}) = \boldsymbol{\partial}_\mathbf{x} . (\bar{\bar{\boldsymbol{\tau}}} . \mathbf{u} + \mathbf{q}^{cond}) + \sigma \lvert \mathbf{E} \rvert^2 + \mathbf{u} . (\mathbf{J} \times \mathbf{B}) - \boldsymbol{\partial}_\mathbf{x} . \mathbf{q}^{rad}$
IMPOSED CURRENT	$\boldsymbol{\partial}_\mathbf{x} . (-\sigma \boldsymbol{\partial}_\mathbf{x} \phi_i) = 0$ $\quad \mathbf{E}_i = - \boldsymbol{\partial}_\mathbf{x} \phi_i$ $\quad \mathbf{J}_i = \sigma \mathbf{E}_i$
IMPOSED MAGNETIC	$\boldsymbol{\partial}_\mathbf{x}^2 \mathbf{A}_i - \mu_0 \sigma \boldsymbol{\partial}_\mathbf{x} \phi_i = 0$ $\quad \mathbf{B}_i = \boldsymbol{\partial}_\mathbf{x} \times \mathbf{Ai}$
EXTERNAL MAGNETIC	$\mathbf{A}_e = \frac{\mu_0 I_e}{4\pi} \oint \frac{\boldsymbol{dl}}{\lvert \boldsymbol{r} - \boldsymbol{r}' \rvert}$ $\quad \mathbf{B}_e = \boldsymbol{\partial}_\mathbf{x} \times \mathbf{A}_e$
TOTAL FIELD	$\mathbf{B} = \mathbf{B}_i + \mathbf{B}_e$ $\quad \mathbf{E} = \mathbf{E}_i$ $\quad \mathbf{J} = \mathbf{J}_i$
RADIATION	$\boldsymbol{n} . \boldsymbol{\partial}_x I_\lambda(\boldsymbol{x}, \boldsymbol{n}) = \kappa_\lambda(\boldsymbol{x}) [B_\lambda(T) - I_\lambda(\boldsymbol{x}, \boldsymbol{n})]$

Efficient Variable Mixture Multi-Band **Radiation** Model [10]

Two major approximations assumed:

- Medium in Local Thermodynamic Equilibrium (LTE)
- Scattering was neglected

NEQAIR was used to calculate the absorption coefficients for variable LTE air-argon mixtures

- F(T, p, χ)
- M++ (equilibrium)
- 13 species (Air13)
- λ = 0.04 - 20 μm
- 550,000 $\Delta\lambda$

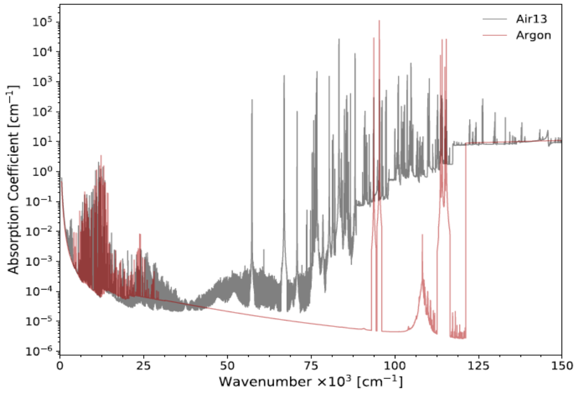

Fig. 1 Spectral absorption coefficients for LTE air and argon at 10,000 K and 1 atm

Radiative Transfer Equation (RTE):

$$\hat{\boldsymbol{n}} \cdot \nabla I_\lambda(\vec{\boldsymbol{x}}, \hat{\boldsymbol{n}}) = \kappa_\lambda(\vec{\boldsymbol{x}}) \left[B_\lambda(T) - I_\lambda(\vec{\boldsymbol{x}}, \hat{\boldsymbol{n}}) \right]$$

Radiative Heat Flux:

$$q(\vec{\boldsymbol{x}}) = \int_0^\infty \int_\Omega I_\lambda(\vec{\boldsymbol{x}}, \hat{\boldsymbol{n}}) \, \hat{\boldsymbol{n}} \, d\Omega \, d\lambda$$

The multi-band method: reduces the spectrum into groups of wavelengths defining a mean absorption coefficient for each group or band:

$$\tilde{\kappa}_b = \kappa_{P_b} = \frac{\int_{\lambda_1}^{\lambda_2} \kappa_\lambda B_\lambda \, d\lambda}{\int_{\lambda_1}^{\lambda_2} B_\lambda \, d\lambda}$$ ➢ **Planck MAC**

$$\tilde{\kappa}_b = \kappa_{R_b} = \frac{\int_{\lambda_1}^{\lambda_2} \frac{\partial B_\lambda}{\partial T} \, d\lambda}{\int_{\lambda_1}^{\lambda_2} \frac{1}{\kappa_\lambda} \frac{\partial B_\lambda}{\partial T} \, d\lambda}$$ ➢ **Rosseland MAC**

$$\tilde{\kappa}_b = \kappa_{BPR_b} = \sqrt{\kappa_{P_b} \, \kappa_{R_b}}$$ ➢ **Blended-PR MAC**

Efficient Variable Mixture Multi-Band **Radiation** Model [10]

Radiative Heat Transfer model:

- **LBL**: very accurate & expensive.
- **Planck and Rosseland**: high error at low number of bands and cost-effective.
- **Blended-PR**: low error at low number of bands and cost-effective.

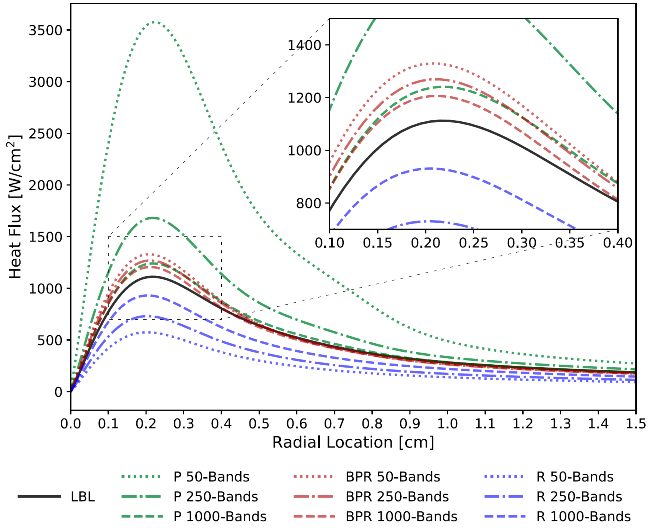

Fig. 1 Heat flux profiles for LBL and different banding models at 10 atm

Variable Air-Argon mixture model:

- Capability to compute variable Air-Argon mixtures on the fly
- Spectral properties of air-argon mixtures can be estimated from air and argon's data.

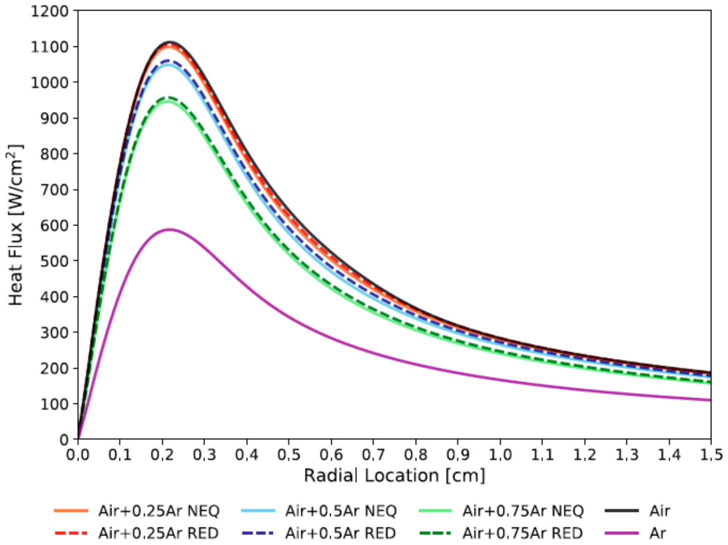

Fig. 2 Heat flux profiles for air-argon mixtures computed LBL and using the reduced model at 10 atm

Efficient 3D radiative transport
advance order method

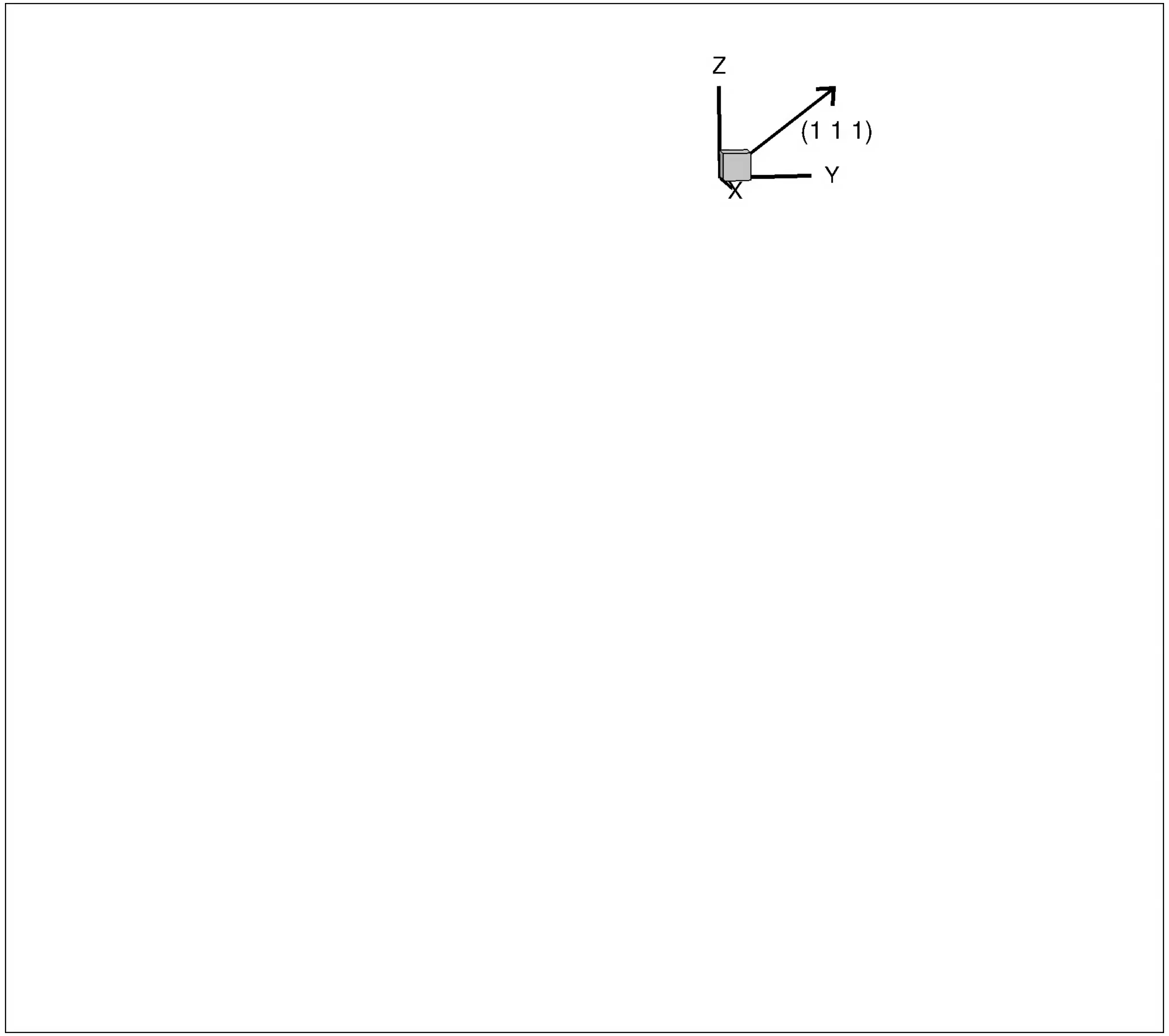

$$I^{d}_{\upsilon,c} = \frac{\sum_{k_i}^{N_{k_i}} I^{d}_{\upsilon,k_i}\, \Omega_d \,.\, \Delta S_c . + \kappa_{\upsilon,c}\; B_{\upsilon,c}\, V_c}{\sum_{k_o}^{N_{k_o}} I^{d}_{\upsilon,k_o}\, \Omega_d \,.\, \Delta S_c . + \kappa_{\upsilon,c}\; V_c}$$

$$\partial_x \,.\, q^{rad} = \sum_{\upsilon}^{N_b} \sum_{d}^{N_d} \frac{a_d\, I^{d}_{\upsilon,c}\, \Omega_d \,.\, \Delta S_c}{V_c}$$

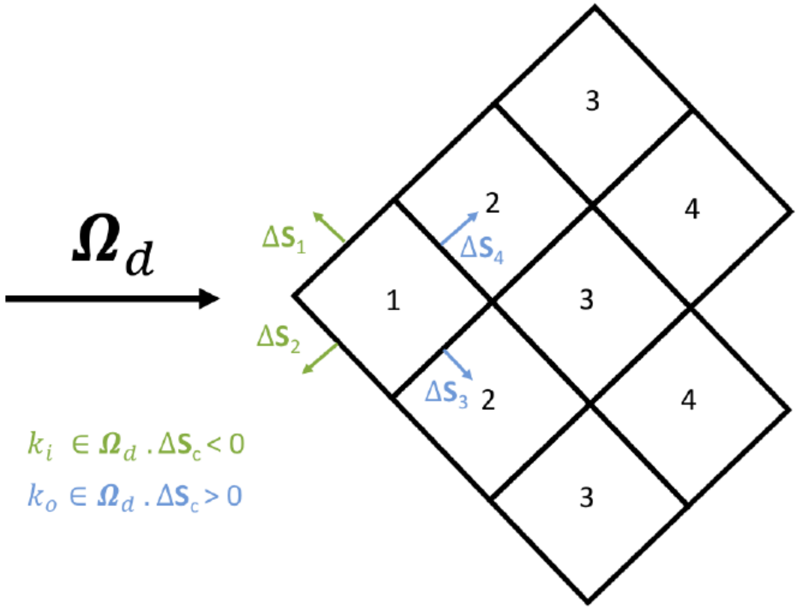

$k_i \in \Omega_d . \Delta S_c < 0$

$k_o \in \Omega_d . \Delta S_c > 0$

Capturing the electric **arc instabilities**

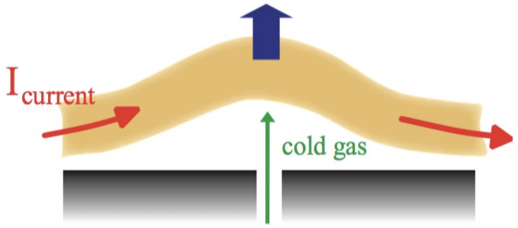

Thermal instability

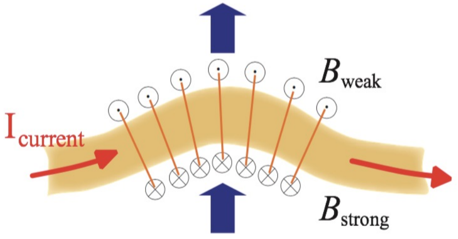

Kink instability

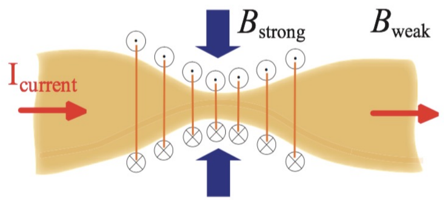

Sausage instability

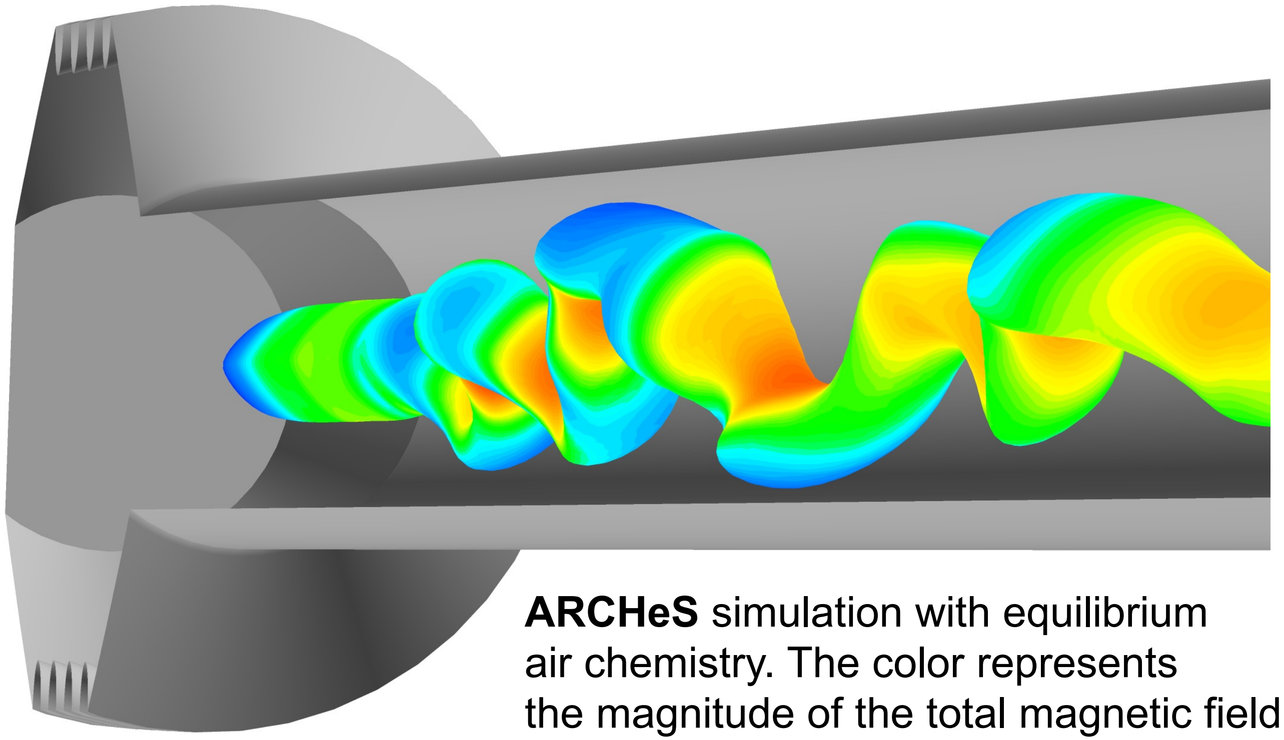

ARCHeS simulation with equilibrium air chemistry. The color represents the magnitude of the total magnetic field. Iso-surface of the current density of 1 MA/m^2.

Stable arc next to the electrode chambers.
Instablilities arise in the constrictor.

Temperature and **radiation** results

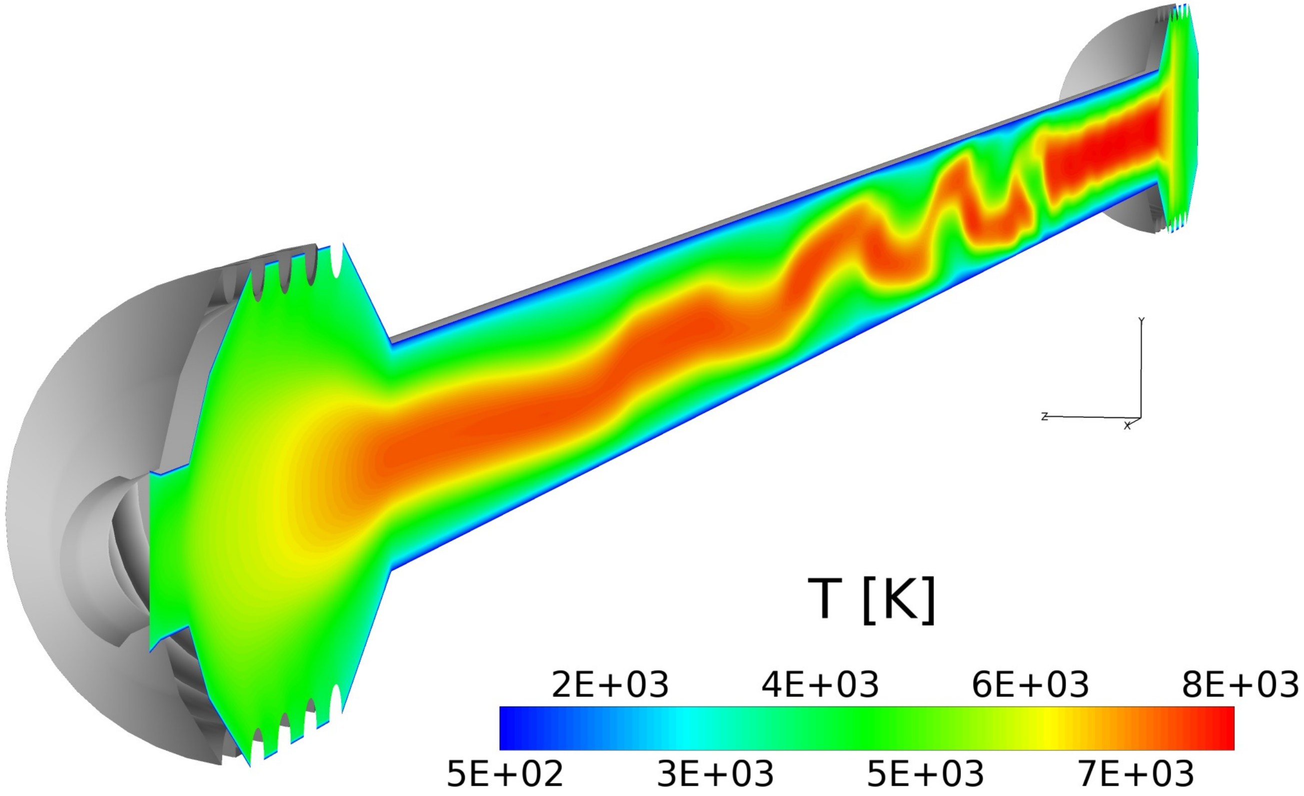

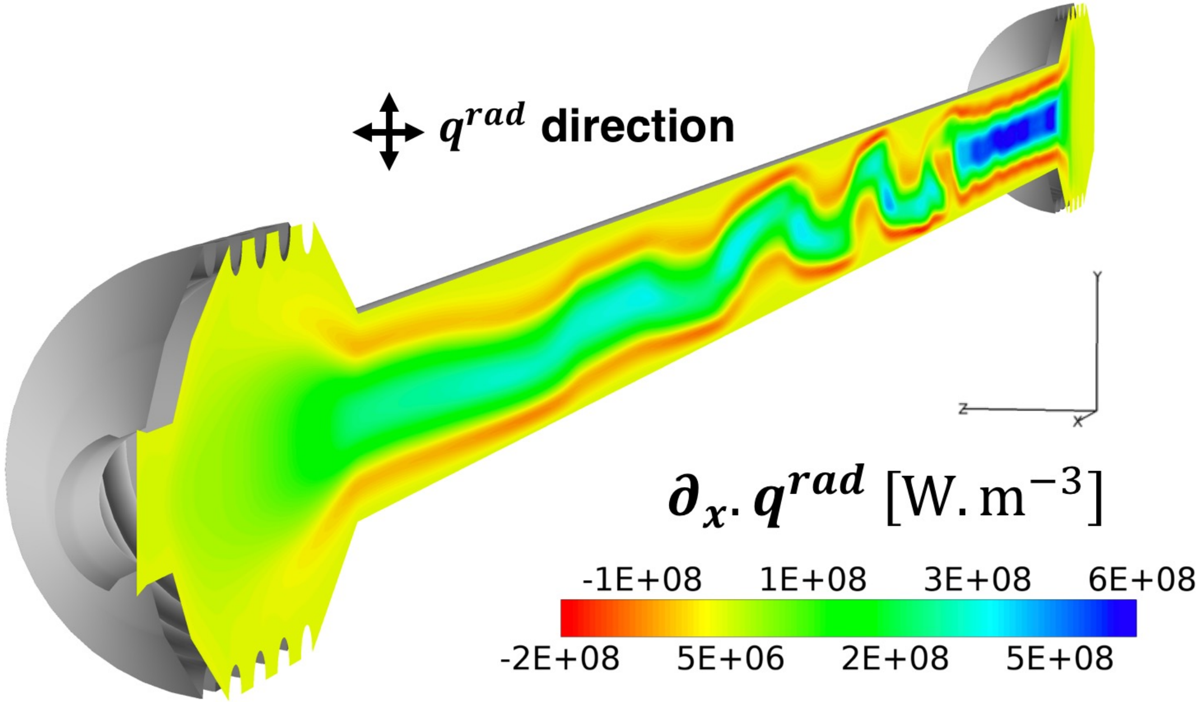

Hot electric arc core cools down and the surroundings warm up.
Importance of the 3D radiative transfer.

Current density and **magnetic field** intensity

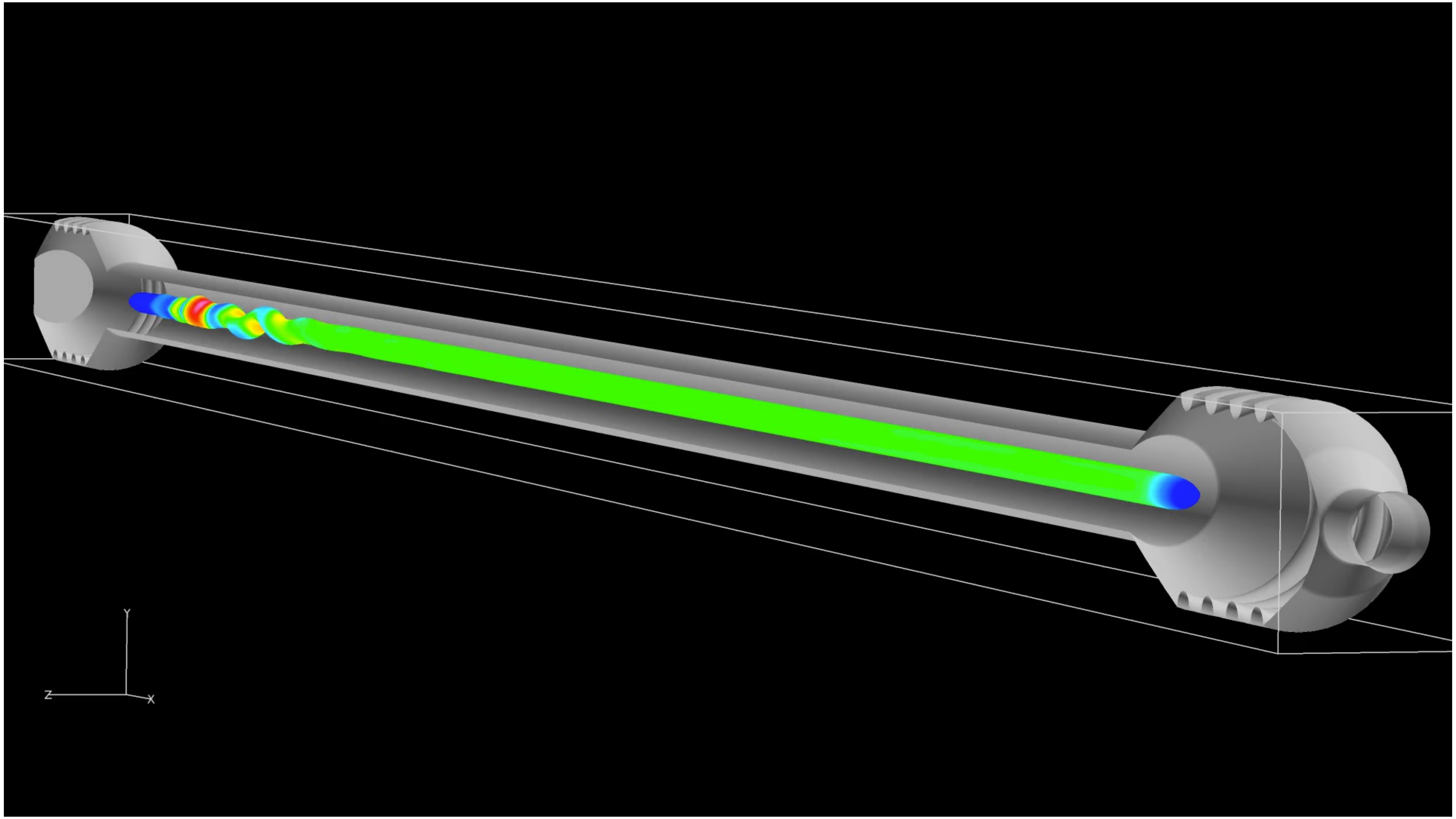

Arc attachment at the electrode

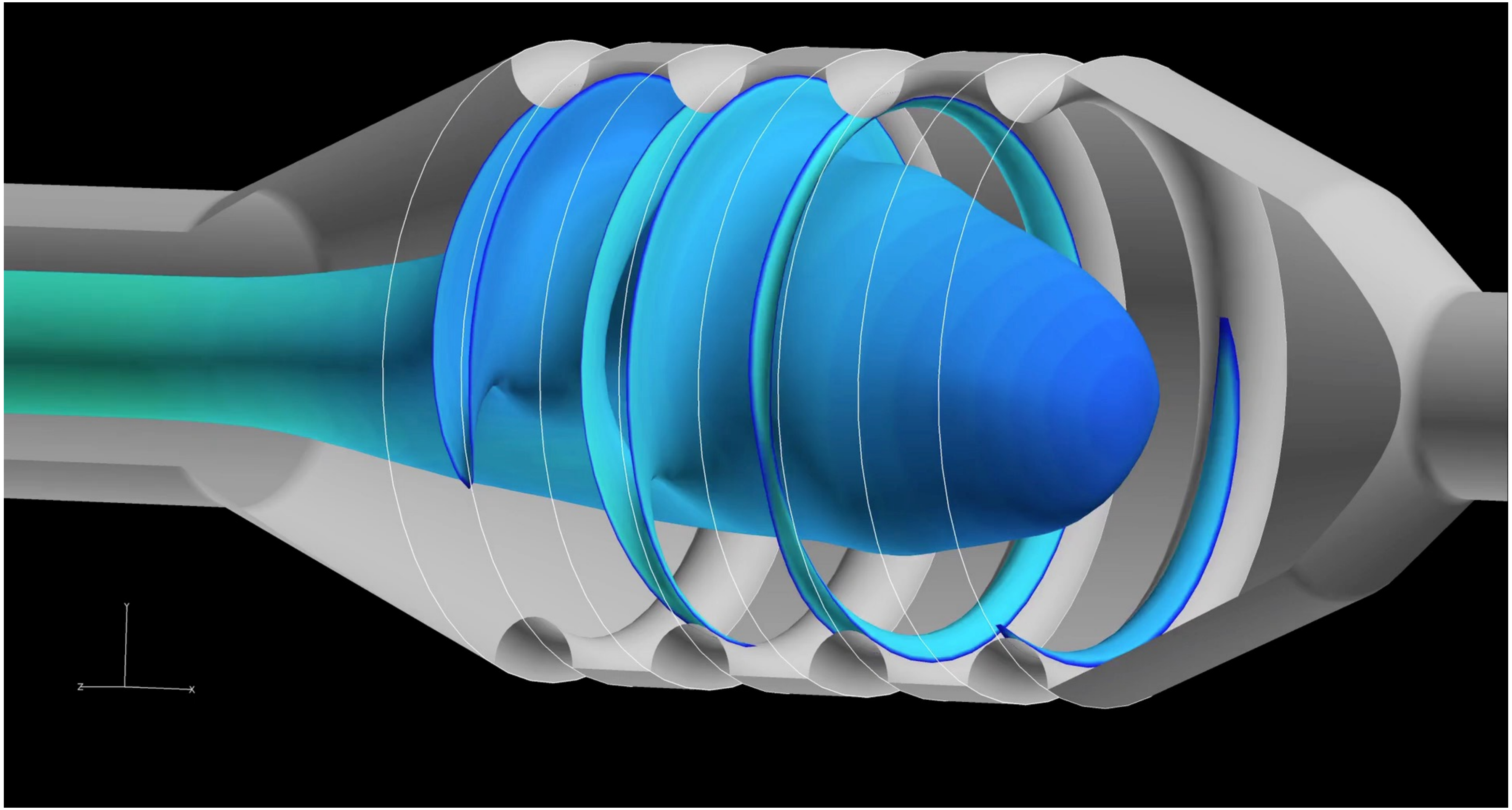

Argon mass fraction

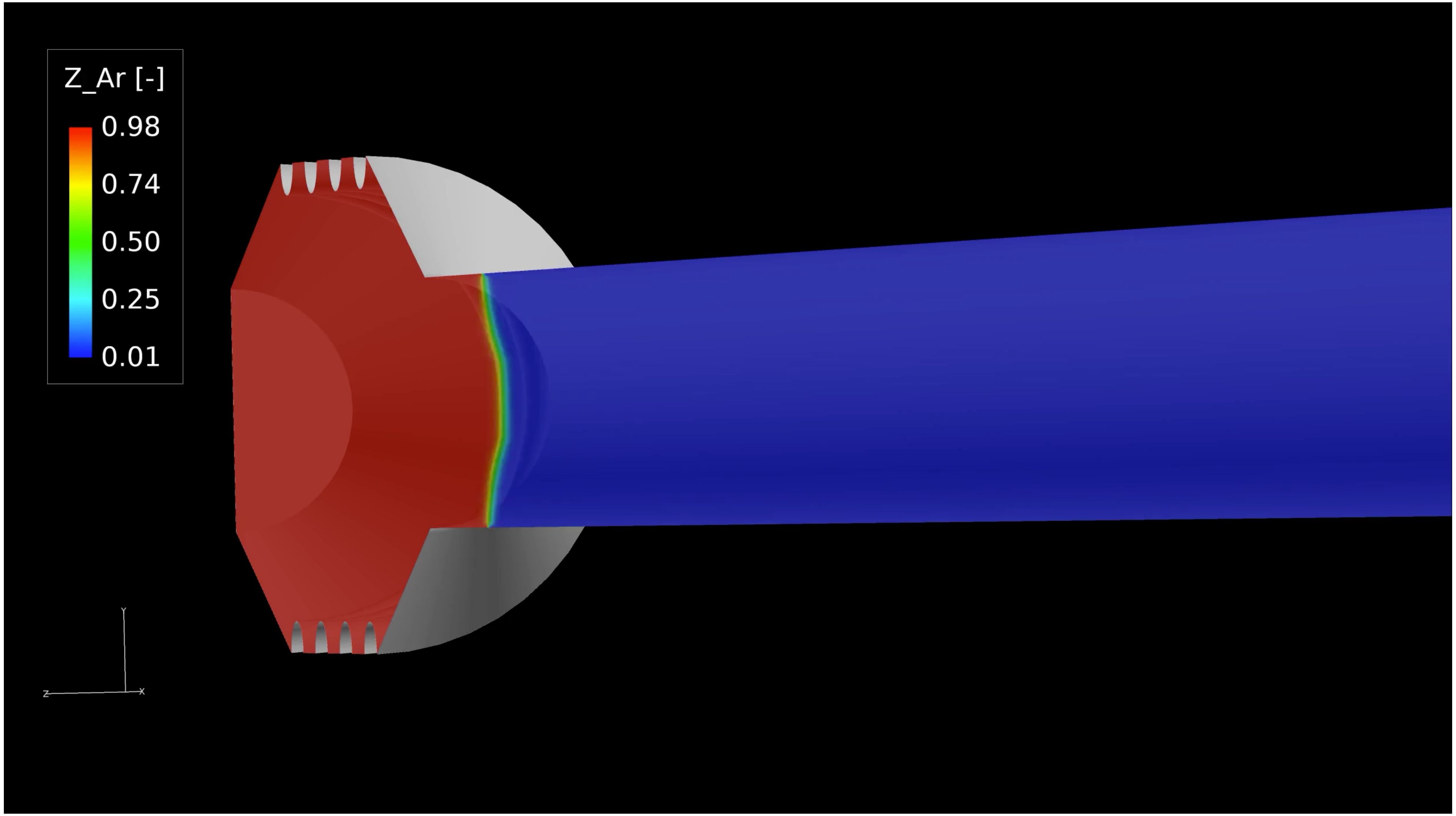

Impact of argon injection on **arc stability**

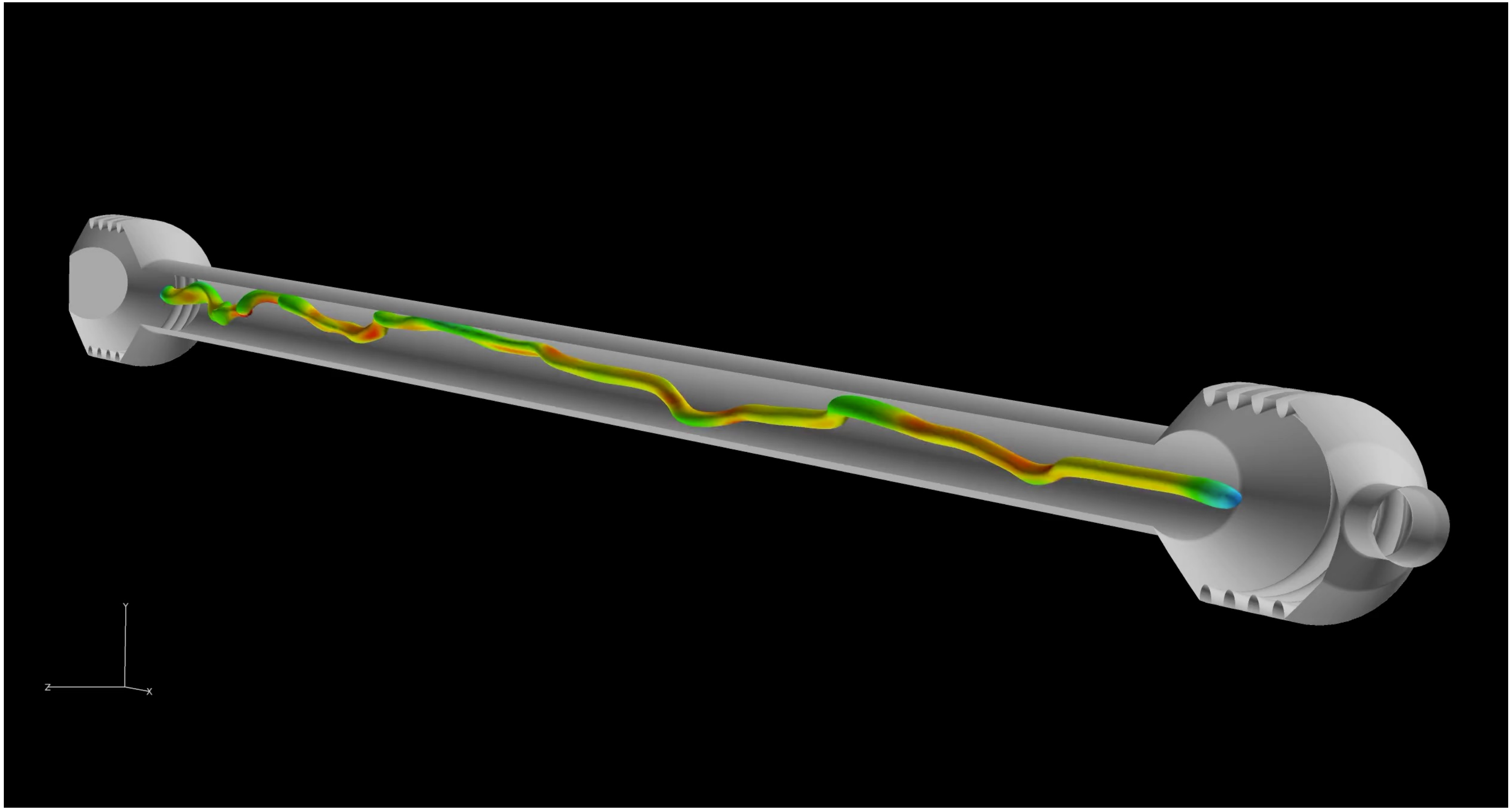

Experimental validation [11]

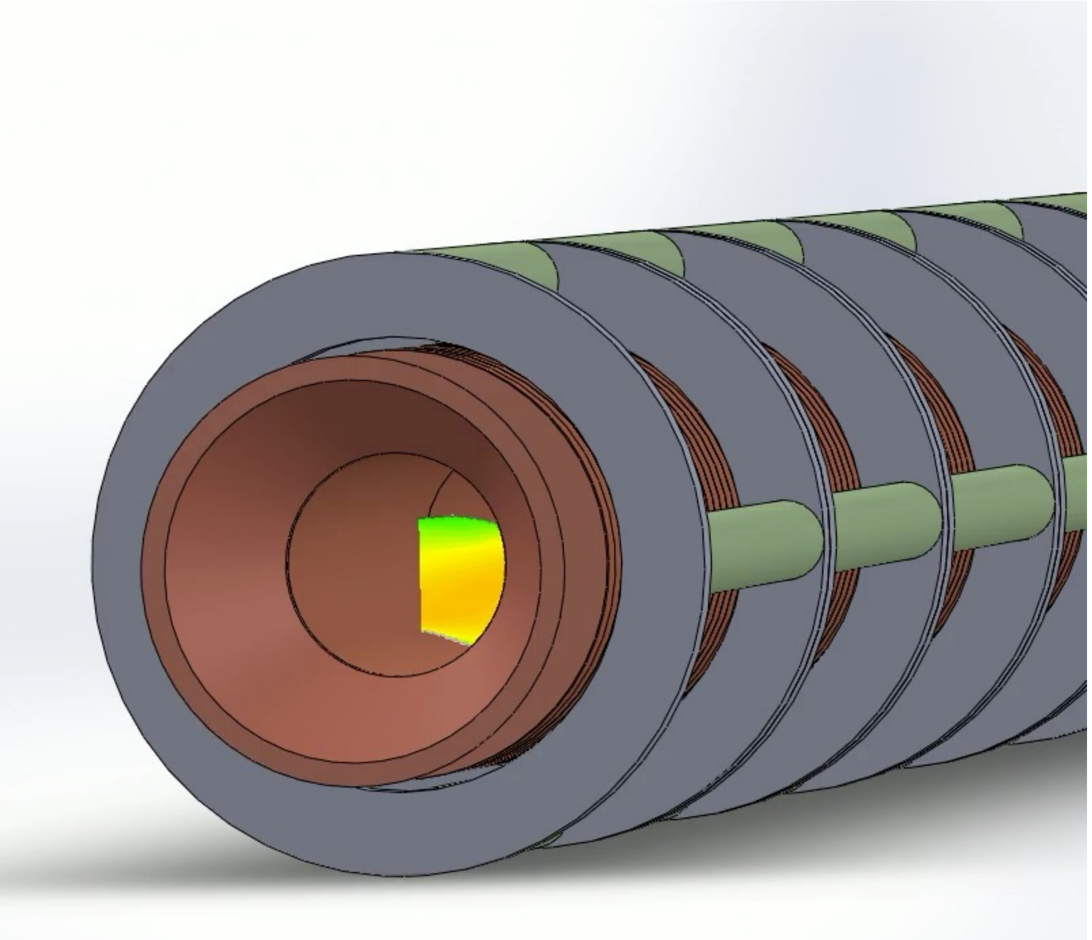

Measurement of Magnetic Kink Instability

AHF TP3 Heater Column (10MW arcjet)

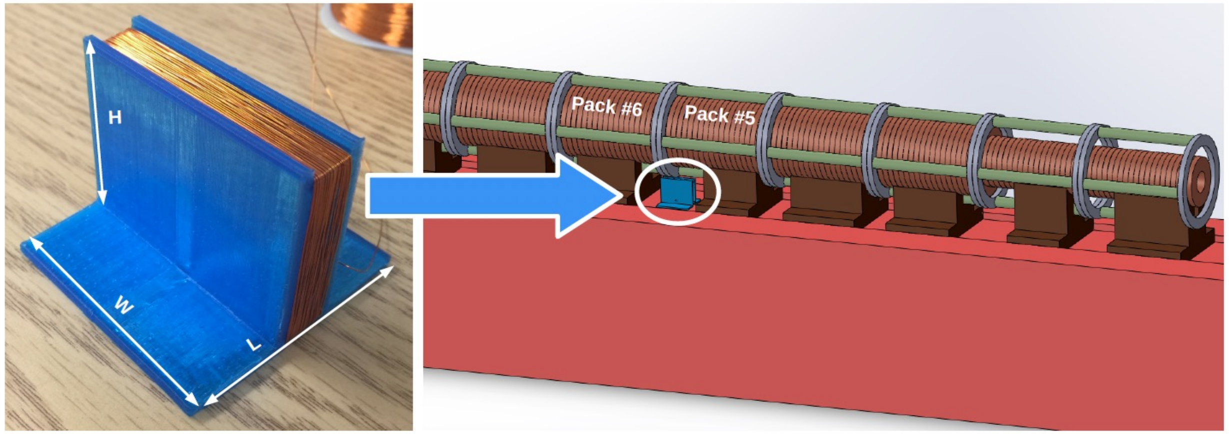

Fig. 1 Image of inductive coil sensor and coil placement below AHF heating column.

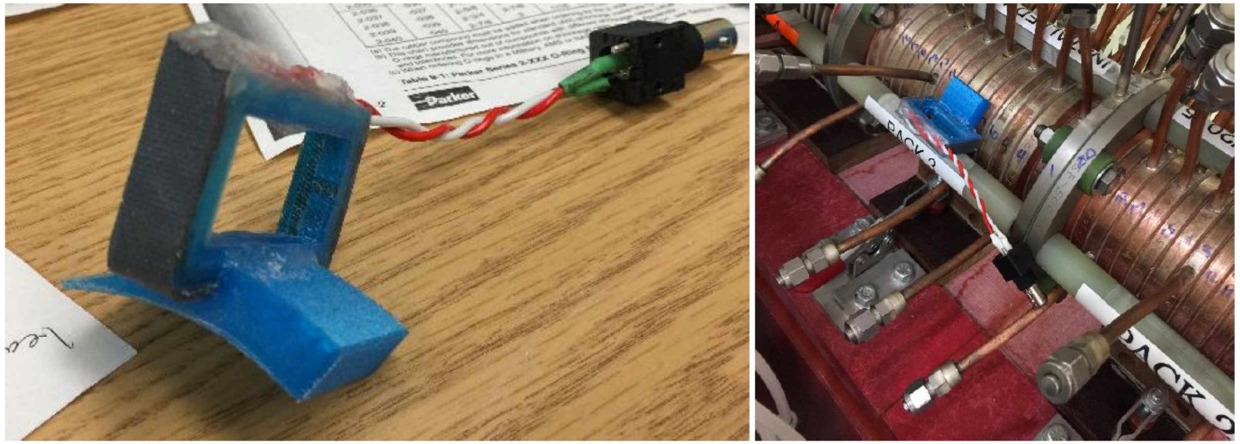

Fig. 2 (Left) Column mounted coil: rectangular coil with 100 turns of AWG 33 wire. 3D printed mount matches curvature of column and thin lower lip fits into the gap between the column and green tension bar. (Right) Coil mounted on Pack 3 of AHF 10 MW heater.

2^{d} part of an arc-jet

High-fidelity modeling of arc-jet aerothermal environments

DPLR

Data-Parallel Line Relaxation

Aerothermal & Hypersonic

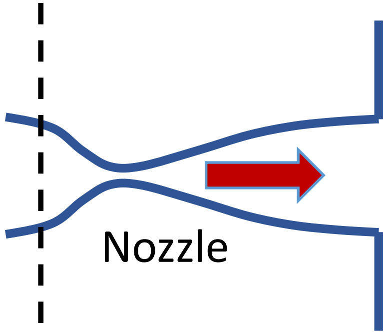

CFD/Machine Learning simulations [12]

Generating database for ML

1. Given $\dot{m}$ for each p_i & h_i
2. **Mutation++:** Compute inflow variables
3. **DPLR**: Stag. point CFD solution each q_w & p_w

ML

4. **Scikit-learn**: Find $[p_i\ ,\ h_i]$ for $q_{w,exp}$ & $p_{w,exp}$

High-fidelity CFD

5. **Mutation++**: Compute inflow variables
6. **DPLR**: Stag. point CFD solution each q_w & p_w
7. **BLAYER**: Compute the BLE envi. C_H, h_e & p_w

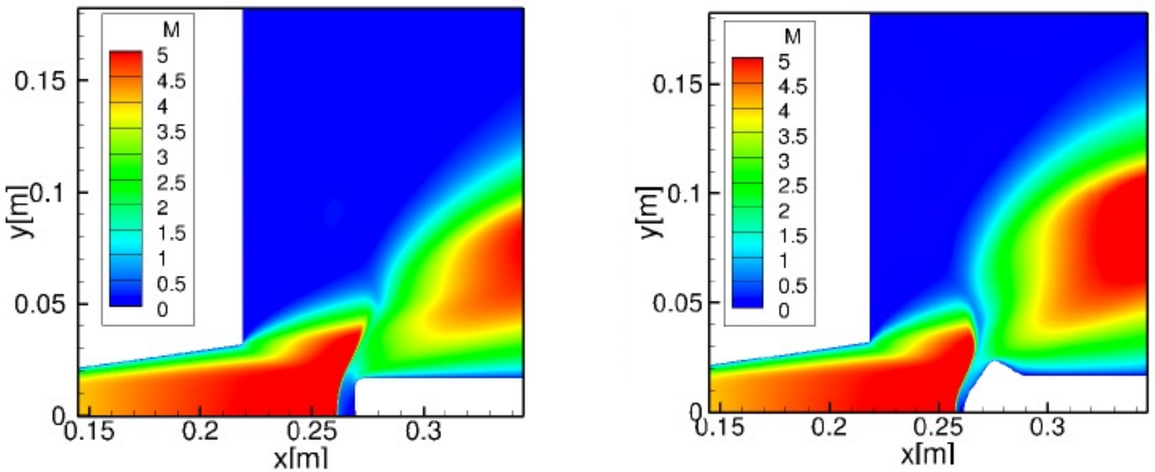

Fig. 1 Mach number contours using Earth atmosphere.

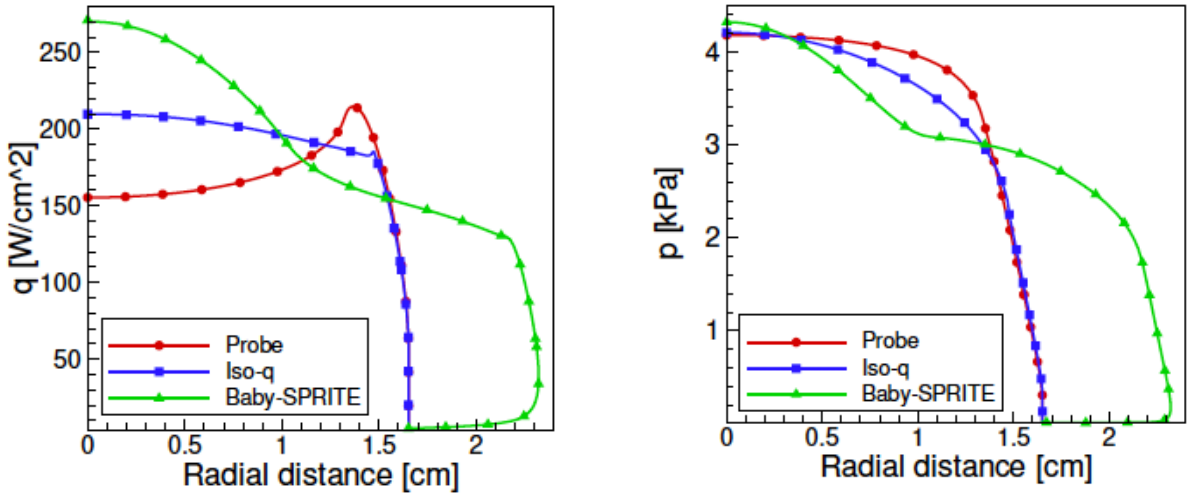

Fig. 2 Distribution of heat flux (left) and pressure (right).

3^d part of an arc-jet
High-fidelity material response modeling

PATO
Porous-material Analysis Toolbox based on OpenFOAM

Material Response

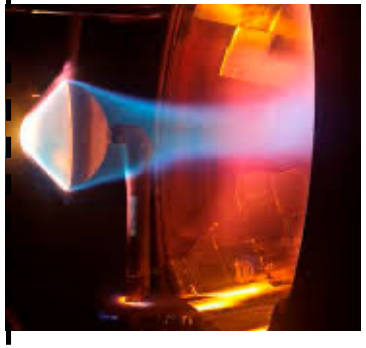

HyMETS test campaign – March 2019 [13,14]

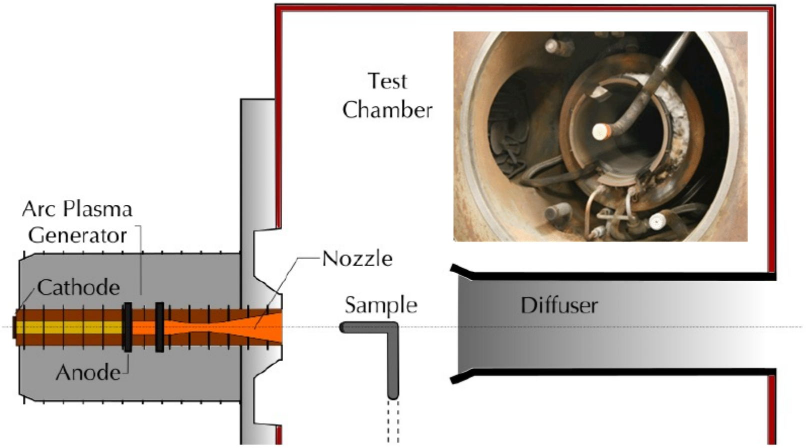

Fig. 1 Schematic view of HyMETS test section. [4]

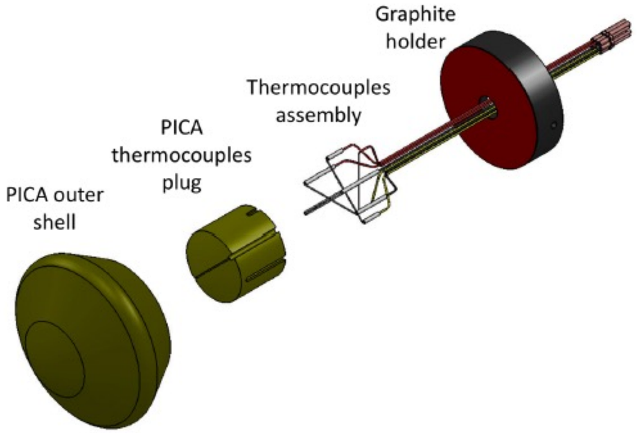

Fig. 2 Baby-SPRITE model assembly.

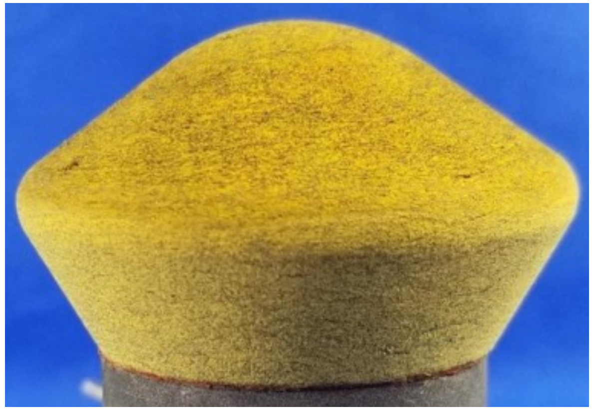

Fig. 3 Baby-SPRITE sample.

Material	Model	Atmosphere	Heat flux [W/cm²]	Pressure [kPa]
PICA-N	1	Earth	140	5.6
PICA-N	2	Earth	140	5.6
PICA-N	3	Earth	140	5.6
PICA-N	4	Earth	60	4.1
PICA-N	5	Earth	224	6.6
PICA-N	6	N_2	131	5.3

Material	Model	Atmosphere	Heat flux [W/cm²]	Pressure [kPa]
PICA-N	7	Mars	127	5.2
PICA-N	8	Earth	60	3.9
PICA	9	Earth	140	5.6
PICA	10	N_2	130	5.3
PICA	11	Earth	223	6.6
PICA	12	Mars	126	5.3

Material response simulations: $\mathbf{CO_2}$ [15,16]

Material	Model	Atmosphere	Heat flux [W/cm²]	Pressure [kPa]
PICA	12	Mars	126	5.3

BLAYER: $p_w = 5.2\ kPa \mid C_H = 0.19 \frac{kg}{m^2 s} \mid h_e = 6.7 \frac{MJ}{kg}$

Recession: $r_{exp} = 5.69\ mm \mid r_{pato} = 6.10\ mm$

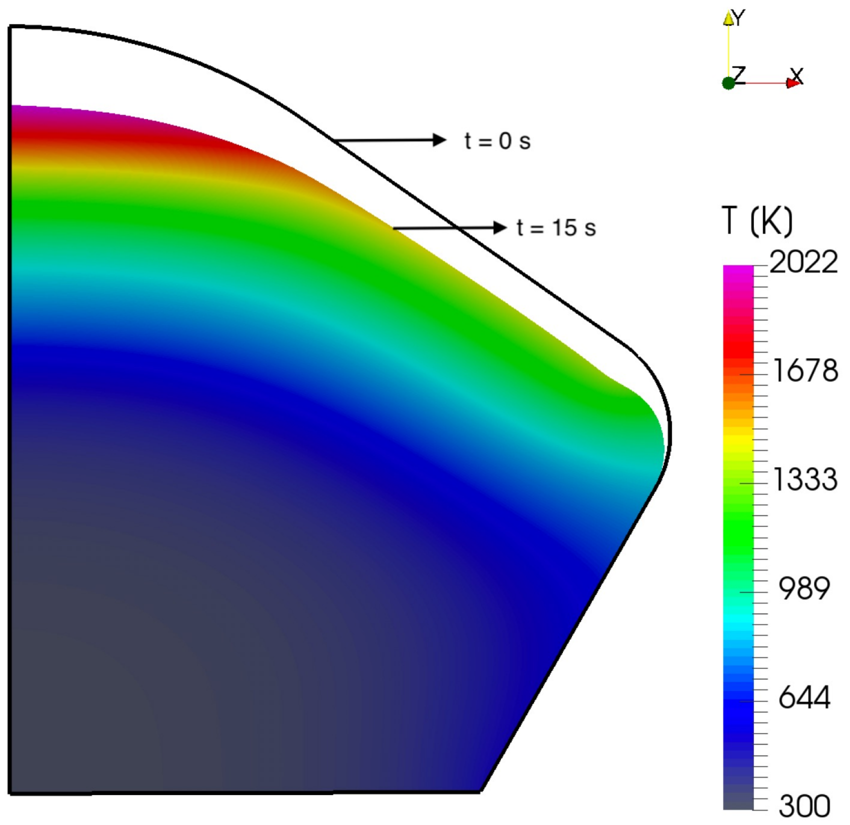

Fig. 1 Temperature and recession at 15 sec.

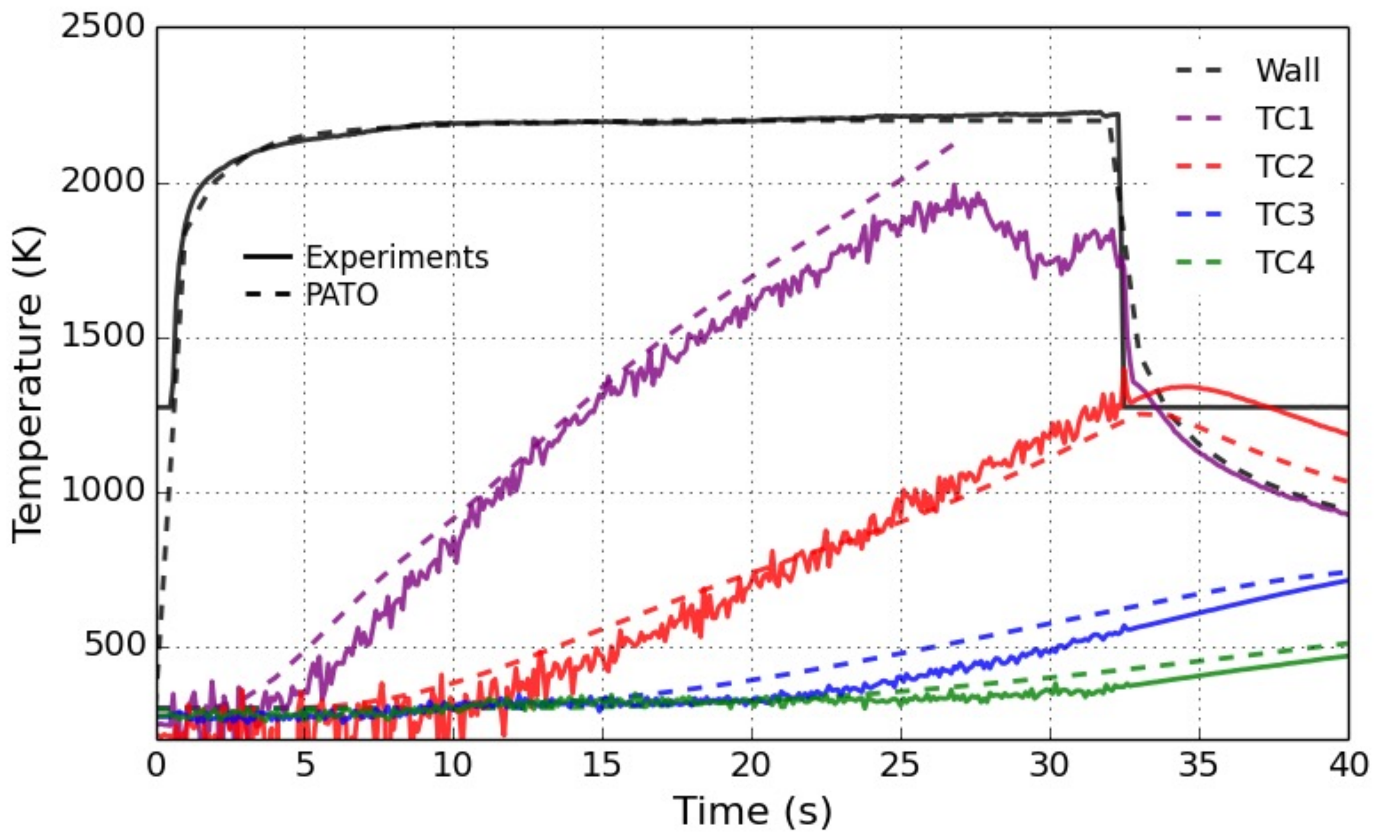

Fig. 2 Evolution in time of the temperature.

High-fidelity modeling of an arc-jet

MHD + 3D radiative transfer

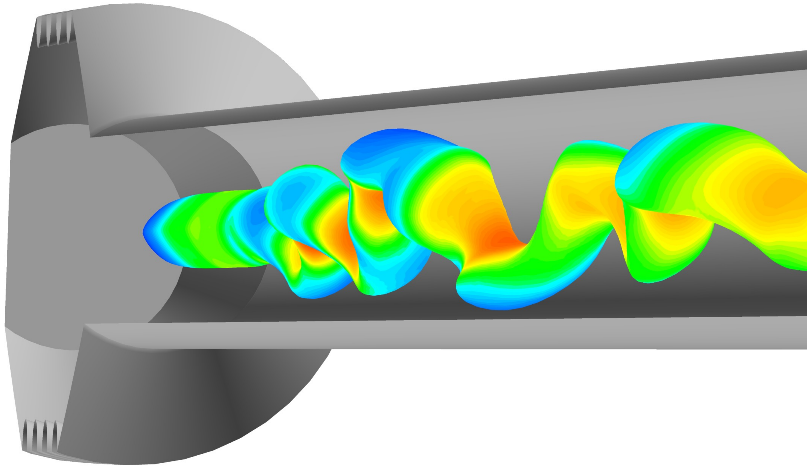

Aerothermal & Hypersonic

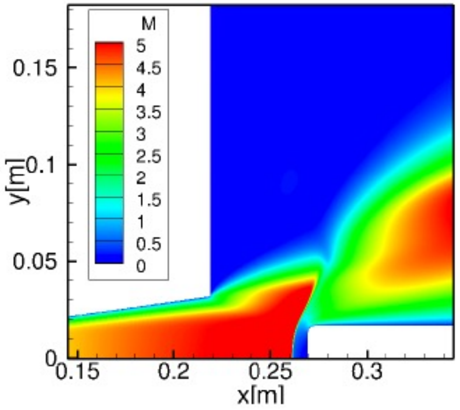

Material Response

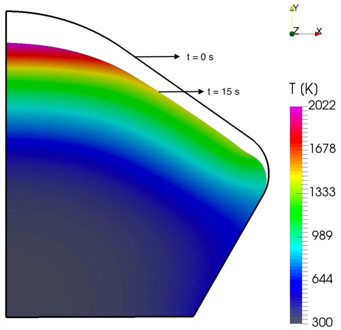

ARCHeS
ARC Heater Simulator

DPLR
Data-Parallel Line Relaxation

PATO
Porous-material Analysis Toolbox based on OpenFOAM

Acknowledgements

- *ARCHeS*: Joseph Schulz, Sander Visser and Alan Wray.
- *DPLR*: Seokkwan Yoon and Almudena Parente.
- *PATO*: Jean Lachaud.
- *VKI*: Andrea Fagnani, Francisco Torres, Joffrey Coheur, and David Henneaux.
- *UIUC*: Przemyslaw Rostkowski, Marco Panesi and Francesco Panerai.
- *ESM*: Aaron Brandis and Michael Barnhardt.

and more

NASA

ILLINOIS
UNIVERSITY OF ILLINOIS AT URBANA-CHAMPAIGN

The von Karman Institute
for Fluid Dynamics

université de BORDEAUX

References

[1] Ferguson, Joseph C., et al. "PuMA: The porous microstructure analysis software." SoftwareX 7 (2018): 81-87.

[2] Semeraro, Federico, et al. "Anisotropic analysis of fibrous and woven materials part 1: Estimation of local orientation." *Computational Materials Science*, 178, p.109631. (2020)

[3] Semeraro, Federico, et al. "Anisotropic analysis of fibrous and woven materials part 2: Computation of effective conductivity." *Computational Materials Science,* 186, p.109956. (2021)

[4] Plimpton et. al, "Direct simulation Monte Carlo on petaflop supercomputers and beyond." Phys. Fluids (2019)

[5] Lachaud, Jean, et al. "A generic local thermal equilibrium model for porous reactive materials submitted to high temperatures." International Journal of Heat and Mass Transfer 108 (2017): 1406-1417.

[6] Lachaud, Jean, et al. "Porous-material analysis toolbox based on OpenFOAM and applications." Journal of Thermophysics and Heat Transfer 28.2 (2014): 191-202.

[7] Meurisse, Jeremie BE, et al. "Multidimensional material response simulations of a full-scale tiled ablative heatshield." *Aerospace Science and Technology* 76 (2018): 497-511.

[8] Torres-Herrador, Francisco, et al. "A high heating rate pyrolysis model for the Phenolic Impregnated Carbon Ablator (PICA) based on mass spectroscopy experiments." Journal of Analytical and Applied Pyrolysis 141 (2019): 104625.

[9] Meurisse, Jeremie, Alejandro Alvarez Laguna, and Nagi Mansour. "3D unsteady model of arc heater plasma flow using the ARC Heater Simulator (ARCHeS)." *APS* (2018): ET1-009.

[10] Fraile Izquierdo, Sergio, et al. "Analysis of Three Multi-Band Models for Radiative Heat Transfer in LTE Air Plasma." AIAA Scitech 2020.

[11] Haw, Magnus A., et al. "Preliminary Measurements of the Motion of Arcjet Current Channel Using Inductive Magnetic Probes." AIAA Scitech 2020.

[12] Ventura Diaz, Patricia, et al. "High-Fidelity Numerical Analysis of Arc-Jet Aerothermal Environments." AIAA Scitech 2020.

[13] Bessire, Brody K., et al. "Progress Towards Modeling The Mars Science Laboratory PICA-Nusil Heatshield." International Planetary Probe Workshop 2019, July 2019.

[14] Bessire, Brody K., et al. "Analysis of the PICA-NuSil HyMETS Arc-Jet Campaign." 11th Ablation Workshop, September 2019.

[15] Ventura Diaz, Patricia, et al. "High-Fidelity Simulations of HyMETS Arc-Jet Flows for PICA-N Modeling" AIAA Scitech 2021.

[16] Meurisse, Jeremie B.E., et al. "Progress towards modeling the ablation response of NuSil-coated PICA." 11th Ablation Workshop, September 2019.